Portable, Stable, and Sensitive Assay to Detect Phosphate in Water with

Gold Nanoparticles and Dextran Tablet

AmirReza Rouhani Esfahani

A Thesis

In the Department

of

Mechanical, Industrial and Aerospace Engineering

Presented in partial fulfillment of the requirements

for the degree of

Master of Applied Science (Mechanical Engineering) at

Concordia University

Montréal, Québec, Canada

November, 2020

CONCORDIA UNIVERSITY

School of Graduate Studies

This is to certify that the thesis prepared

By: AmirReza Rouhani Esfahani

Entitled: **Portable, Stable and Sensitive Assay to Detect Phosphate in Water with Gold Nanoparticles (AuNPs) and Dextran Tablet**

And submitted in partial fulfilment of the requirements for the degree of

Master of Applied Science (Mechanical Engineering)

Complies with the regulations of the University and meets the accepted standards with respect to originality and quality.

Signed by the final Examining Committee:

_____ Chair

Dr. Ramin Sedaghati

_____ Internal Examiner

Dr. Ramin Sedaghati

_____ External Examiner

Dr. Chunjiang An

_____ Thesis Supervisor

Dr. Sana Jahanshahi-Anbuhi

Approved by: _____

Dr. Mamoun Medraj, Graduate Program Director

Date _____ 2020   _____ Dean of Faculty

Dr. Mourad Debbabi

Abstract

Portable, Stable, and Sensitive Assay to Detect Phosphate in Water with Gold Nanoparticles and Dextran Tablet

AmirReza Rouhani Esfahani

Phosphate (Pi) is a necessary element for growth and energy transport in humans, animals and plants. However, the excess amount of this element could cause severe problems such as joint pain and skin rash for humans and eutrophication in nature. Eutrophication is the enrichment of nutrients, especially phosphate, in aquatic systems, with harmful effects on surface water bodies, such as lakes and creatures in the water.

This thesis investigated the applicability of gold nanoparticles to detect phosphate using different methods including paper-based and tablet-based sensors. A novel and highly sensitive tablet-based colorimetric sensor is developed to detect phosphate (Pi) in water using mercaptoacetic acid-gold nanoparticles (MA-AuNPs). The principle of this sensor is based on the aggregation (blue colored) and disaggregation (red-colored) mechanism of AuNPs due to surface plasmon resonance, where europium ions (Eu^{3+}) act as an aggregating agent. Herein, dextran

tablets encapsulated the Eu^{3+} ions to make the detection system user friendly. Hence, the sensor just requires dissolving the Eu^{3+}-dextran tablet into the water sample and subsequently adding MA-AuNPs for the colorimetric quantification of phosphate. This assay is very sensitive, with a calculated lower detection limit of 3.779 µg/L and upper detection limit of 0.328 mg/L. The assay does not interfere with common ions in water, thus being Pi-specific, and the display results were stable up to three weeks. Overall, this new approach provides a simple, stable, rapid, low cost and promising device for Pi detection in water.

List of publications and conference contributions

- **A. R. Esfahani**, Zubi Sadiq, Oyejide Damilola Oyewunmi, Ndifreke Usen, Daria Camilla Boffito, Sana Jahanshahi-Anbuhi "Portable, stable and sensitive assay to detect phosphate in water with gold nanoparticles (AuNPs) and dextran tablet", *Analyst journal,* Under Review, **2020**

- **A. R. Esfahani**, S. Jahanshahi-Anbuhi "Colorimetric sensor for detection of phosphate ions using gold nanoplates and europium ions" *BIOFOR International Conference*, Montreal, Canada; February **2020**

- **A. R. Esfahani**, S. Jahanshahi-Anbuhi, Ndifreke Usen, Daria Camilla Boffito, "Colorimetric sensor for determination of nitrate ions using gold nanoparticles" *CQMF-QCAM Student Symposium*, Montreal, Canada; November **2019**

- **A. R. Esfahani**, S. Jahanshahi-Anbuhi "Paper-based biosensors with gold nanoparticles for phosphate detection in the water" *Chemical and Materials Engineering Research Day*; University of Polytechnique Montreal; March **2019**

Acknowledgment

First and foremost, I would like to express my sincere gratitude to my supervisor, Dr. Sana Jahanshahi-Anbuhi for believing in me and for giving me the opportunity to be a part of her research group. I am grateful for her continuous support and encouragement during the course of my master's program. I have immensely learned from not only her invaluable scientific input and academic advice, but also from her aspiring life lessons, creativity, compassion and commitment. It has been a great privilege to work and learn from her. I wish to thank my labmate, Dr. Zubi Sadiq, my great colleague, who acted as a lab supervisor for me. She always helped me through difficulties of the research, and we managed to have a great teamwork experience.

1 would like to express my thanks to Dr. Daria Camilla Boffito for her helpful supports and advice on my project. Also, I appreciate Ndifreke Usen for the comments and suggestions to enrich my research. Moreover, I want to thank Mr. Masoud Aminzare for his invaluable help in characterization of the gold nanoparticles.

Contents

List of figures

List of tables

Abbreviation and symbols list

Abbreviation	Meaning
WHO	World health organization
Pi	Phosphate
μPADs	Microfluidic paper-based analytical devices
AuNPs	Gold nanoparticles
MNPs	Metal nanoparticles
NPs	Nanoparticles
MA-AuNPs	Mercaptoacetic acid gold nanoparticles
MA	Mercaptoacetic acid
Au	Gold
Ag	Silver
°C	Degree of Celsius
DI	De-ionized water
NaCl	Sodium chloride

UV-Vis	Ultraviolet light visible
UV	Ultraviolet
TEM	Transmission electron microscopy
λ	Wavelength
sec	Second
min	Minutes
h	Hour
g	Gram
mL	Milliliter
mg	Milligram
mM	Millimolar
µg	Microgram
µM	Micromolar
µmol	Micromole
mmol	Millimole
mol	Mole
Wt	Weight

Na	Sodium
HCl	Hydrochloric acid
HNO3	Nitric acid
rpm	Round per minutes

Chapter 1. Introduction

In this chapter a brief introduction for water pollution and detection of phosphate in water is presented. This section continuous with the objectives of this research project and ends up with the thesis outline.

1.1. Background

The pioneering work in the area of gold nanoparticles (AuNPs) was initiated by Michael Faraday in the 1850s when he accidentally created a ruby red colloidal gold [1]. Since then, researchers have investigated its synthesis, properties and potential applications in different fields, including drug delivery [2,3], sensors [4,5], air purification [6], solar cells [7,8], catalysis [9], photocatalysis [10], etc. More recently, AuNPs have been reported for onsite detection applications, specifically, in sensor systems to monitor water quality by identifying and quantifying various ions including arsenic [11], mercury [12], lead [13], copper [13], nitrate [14], fluoride [15] and phosphate [16]. The quantification is often achieved through colorimetric outputs which have been widely used in various analytical platforms [17–19]. The quantification of phosphorus in water is a common quality parameter. This is due to the importance of phosphorus to aquatic life for growth and energy transfer [15,16]. Many countries around the world regulate both the phosphorus removal requirements and the maximum concentration of acceptable phosphorous in the wastewaters. Typical values are less than 1 mg/L or 1 ppm for wastewater, but more and more new European regulations are setting the new limit to 0.01 mg/L [20].

The primary sources of phosphorus are the terrestrial and aquatic environments through soil and bank erosion, in which the phosphorus cycle naturally regulates the amount of this element in the ecosystem [21]. However, phosphorus is also a typical component of fertilizers, manure,

and it is also found in municipal solid waste, as well as in sewage and industrial effluent wastewaters. The illegal human disposal of both toxic waste and waste from factories contribute to phosphorous runoff into water bodies and deep in the soil, which significantly increases the amount of this element in the aquatic habitat [18,19]. Therefore, even a moderate increase in phosphorus concentration has the power of setting off a variety of enchained hazardous effects to the aquatic environment, including algae boom, leading to the suffocation of aquatic animals by decreasing the dissolved oxygen, which ultimately causes death. This process of algae boom is called eutrophication [20,22], and leads to the formation of biotoxins in water [23], including venerupin poisoning (VP) [24], diarrhoetic shellfish poisoning (DSP) [24], alexandrium fundyense [25], dinophysis acuminate [25], neurotoxic shellfish poisoning (NSP) [24], and paralytic shellfish poisoning (PSP) [30]. In addition, phosphorus in drinking water may cause rashes on the skin, joint pains, and kidney malfunction [26]. Therefore, the amount of phosphorus in the form of dissolved phosphate in water is an essential factor in water quality. The common methods for the detection of phosphate and phosphorous in a solution include the electrochemical technique [27,28], the surface-enhanced raman scattering (SERS) [23,24], and the complexometric back titration method [29]. These techniques are expensive, labor-intensive, and require a continuous power source and bulky equipment. These challenges limit the use of these testing techniques in resource-limited regions and developing countries.

1.2. Objective

Despite the extensive research conducted in the field of ion detection with gold nanoparticles and optimizing its sensitivity and applicability, limited research has been done on utilizing the gold nanoparticles for the phosphate detection. This study was mainly focused on the performance of a paper-based and tablet-based sensor for detection of phosphate in water. That

said, the overarching objective of this study is to optimize the functionalized gold nanoparticles and fabricate an easy-to-use sensor. The sub-objectives of this study were to:

- Synthesis and characterization of spherical gold nanoparticles (AuNPs) with the Turkevich method and their functionalization with mercaproacetic acid (MA) to make them sensitive to phosphate and europium ions.
- Examination of the effect of tris-buffer HCl on the applicability, sensitivity, and stability of the functionalized MA-AuNPs in the process of phosphate detection.
- Fabrication of a paper-based device using MA-AuNPs and Eu^{3+} and examination of its performance in detection of phosphate ions in the water.
- Fabrication of a tablet-based device using MA-AuNPs and Eu^{3+} and examination of its performance in detection of phosphate ions in the water.

1.3. Thesis outline

The present thesis document has five chapters in the following structure:

Chapter 2 contains a comprehensive literature review on gold nanoparticles, its chemical and physical properties, and its synthesis methods. Moreover, water pollutants and eutrophication have been discussed in this chapter. Chapter 3 focuses on the chemicals and methods, the synthesis and functionalization of gold nanoparticles, and paper and tablet preparation. Chapter 4 presents the obtained results and the commensurate discussions. As a final point, the conclusions of the work and suggestions for future research are specified in Chapter 5.

Chapter 2. Literature Review

In this chapter some general information is provided about the gold nanoparticles including its chemistry and physical properties and different methods of synthesis. This part continuous with an overview on water pollutants and ends up with eutrophication and different lake types.

2.1. Nanotechnology and nanoscience

Albert Einstein published an experimental data in 1905 showing that the diameter of a single sugar molecule to be 1 nm and initiated the nanotechnology [30]. Nanoscale science began in 1959, when physicist Richard Feynman presented a famous speech named "There is Plenty of Room at the Bottom" and won the Nobel Prize, therefore presenting nanotechnology for the first time. He noted that "someday it would be possible to put the entire 24 volumes Encyclopedia Britannica on the head of a pin" [30]. Dr. Feynman attracted his audience attention to biological cells and mentioned that "although cells are very tiny, they are very active; they manufacture various substances; they walk around; they wiggle, and they do all kinds of marvelous things all on a very small scale" [31]. Also, he pointed out that computing machines could be miniaturized to a very small scale to simulate the properties of small-scale structures. The atomic force microscope (AFM) and the scanning tunneling microscope (STM) was discovered by Gerd Binnig and Heinrich Rohrer in the IBM Research Centre located in Zurich in the 1980s, and these devices enabled the research into the study of nanotechnology due to their unprecedented power to capture images at an extremely low magnification [31]. About six years later, in 1986, Eric K. Drexler published the first book about nanotechnology titled "Engines of Creation: The Coming Era of Nanotechnology" and talked about the future of nanoscience.

In summary, nano can be described as "extremely small or one-billionth"; therefore, the scale is nanometer. Nanotechnology is based on the capability to manipulate, control and reduce atoms and molecules to smaller segments, systems and devices. In other words, at the small scale, materials have special physical and chemical features, which have a great potential for different applications such as drug delivery [3,32], detection [33,34], solar cells [7,35], etc.

2.2. Gold nanoparticles

Gold nanoparticles (AuNPs) have been used since ancient times to make stained-glass in sacred places, including churches. It was long assumed that the color of the gold suspension was as a result of the chemicals used to prepare it. In 1857, Michael Faraday discovered the relationship between gold particle size and its color by synthesizing the first pure gold colloid [36].

Colloidal gold solutions are made of sub-micrometer-sized particles dispersed in a liquid. AuNPs are corrosion and oxidation resistant, which make them applicable for the environment or aqueous experiments. Gold in the nanoscale attracts scientist's attention as it became clear that their bulk properties change as the size decrease from micro-sized materials to small atomic clusters. The higher relative surface area and the dominance of size-dependent properties come from size reduction, impact to the nanoparticles' special electrical [37], thermal [38], and optical characteristics [39] as well as chemical reactivity. Hence, specific nanoparticles dimensions for different kind of metals can be fabricated. However, Michael Faraday, the pioneer in the discovery of the colloidal metal nanoparticles' nature, presented size reduction has some difficulties as the nanoparticles tend to aggregate in order to reduce their surface energy [36]. He noticed the AuNPs in solution were thermodynamically unstable and necessitated kinetic stabilization to prevent their aggregation. The commonest methods of stabilization involve the introduction of chemical agents, before or during the synthesis, which creates a protecting shell around the nanoparticles that

prevent particle aggregation by electrostatic repulsion or steric hindrance. Besides stabilizing the particles, these chemicals act as functionalization agents which can prepare the NPs to be used for different applications such as self-assembly and electrostatic [16].

2.3. Gold chemistry

Many experimental and theoretical methods have been presented to examine and rationalize interactions between gold-ligand. As gold stabilization takes place by linking capping molecules containing functional groups such as amine, alcohol, thiol and phosphines, understanding these surface phenomena is necessary. Among different methods, the broad range of interaction strengths given by these ligands can be specified by Pearson's hard/soft-acid/base (HSAB) theorem, which classifies chemical interactions in terms of hard and soft acid-base interaction according to particular parameters [40]. Because the idea was proven for bulk material, in the case of ligand to metallic nanoparticle connections, the validity of the concept in a microenvironment was recently validated.

The definition of the HSAB mandates that hard acids choose hard bases and soft acids choose soft bases. [40]. The following four statements illustrate such behavior: 1) different degrees of ionic-covalent, 2) solvation effect 3) electron-correlation 4) σ-binding. The Au atom which comprising the metallic nanoparticle surface is called a soft acid, because of its low valence state. This represented as a large polarizable atom with low or partial positive charge, having electron pairs in its valence shells and low LUMO energy. Hence, the soft acid will complex readily with a number of corresponding soft bases that have identical polarizability features (low electronegativity) and sizes [41,42]. The two separate bases groups are described in Table 1.

Table 1 Classification of Lewis Bases and their definitions (adopted from Refs. [40]).

Hard	**Soft**
- Small atoms, highly solvated	- Large atoms of intermediate electronegativity
- Weakly polarizable	
- Difficult to oxidize	- Easily polarizable
- High energy HOMO	- Easy to oxidizes
	- Low energy HOMO
H_2O, OH^-, F^-	R_2S, RSH, RS^-
$CH_3CO_2^-, PO_4^{3-}, SO_4^{2-}$	I^-, SCN^-, RS^-
Cl^-, CO_3^{2-}, ClO_4^-	$R_3P, R_3AS, (RO)_3P$
ROH, RO^-, R_2O	CN^-, RNC, CO
NH_3, RNH_2, N_2H_4	C_2H_4, C_6H_6, H^-, R^-
Borderline (intermediate properties)	
$C_6H_5NH_2 , C_5H_5N, N_3^-, Br^-, NO_2^-, SO_3^{2-}, N_2$	

Based on the Table 1, it is expected that AuNPs and sulphur interact intensely, which is a soft base and a weaker interaction with hard acid RNH_2. The theory is that softer basic ligands are supposed to interact with the metal with an electron donation procedure from their lone pair of electrons available to metal surface. Also, lab experiments studies support the assumption, as thiols

have been found to bind strongly to gold particles by covalent bonding and cause substantial redistribution of surface charge. However, amines show poor tendencies to AuNPs as they weakly associate with the metal without changing its electronic features. It is worth understanding that there are certain variations to the HSAB classification, and it is not absolute, but it can rather be used as a useful method to estimate Lewis acid-base reaction. The nature of the ligand's binding to AuNPs is also determined by the bonding symmetry, in addition to the Lewis basic character [43], the crystallographic face of the metal, and the ability of the ligand to induce the back-bonding. In this procedure, electrons in the d-orbital of the metal are donated to the anti-bonding molecular orbital of a π-acceptor ligand, which relives the excess negative charge of the metal and causes the metal-ligand bond order to increase. These interactions have been shown to play a significant role in the stabilization of oxyanions by AuNPs. These ionic ligands have been shown to coordinate metal surfaces through both electrostatic interactions of the anion and coordination of the oxygen donor atom. Oxyanions with back-bonding d-orbitals have shown a better ability to stabilize the colloidal structure. The order of thermodynamic equilibrium, which differs with the force of back-bonding, was also observed to obey this pattern: CO_3^{2-}<$H_2PO_4^-$<SO_4^{2-}. Despite their poor gold affinity, the ability to stabilize gold nanoparticles suspended in an organic solvent has also been shown by chlorine and bromine ions. Although they tend to cause nanoparticle coagulation by electrostatic neutralization in the polar solvent, when ionically coupled to the counterion of a bulky hydrophobic molecule, these ions may serve as efficient phase transfer agents from aqueous to the organic solution. In the polar phase, the ionic pair stabilizes the nanoparticles, while the non-polar component creates steric repulsions that cause the suspension to be moved to the organic phase. AuNPs can therefore be stabilized by a wide range of interaction mechanisms whose degree of efficiency depends primarily on the existence of the ligand's binding to gold [44].

2.4. Physical properties
2.4.1. General properties

Gold nanoparticles can be synthesized to various morphologies like rods [45], cubes [46], pyramids [47] and prisms [24], etc. The typical shape for AuNPs are spherical without pronounced facets in the range of 5-30 nm [49].

Highly faceted morphologies are synthesized when a capping agent that has a possibly ineffective capping interaction with the nanoparticles is used. However, high resolution-transmission electron microscopy (TEM) images have revealed Au cores with spherical shapes, also have small facets, exhibiting different geometrical projections of a truncated octahedron. Moreover, AuNPs assemble in a crystalline packing with <111> faces are demonstrated using X-ray diffraction[50]. Due to the quantum confinement of their electronic states, AuNPs small nanoclusters possess size-dependent chemical and physical characteristics. For instance, gold which is chemically inert in the bulk state becomes highly reactive in the nanoscale range. Indeed, AuNPs have shown valuable catalytic potential for CO and H_2 oxidation, NO reduction, CO_2 hydrogenation and for the combustion of methanol. Moreover, thermodynamic properties of gold change with its dimension as its melting temperature enormously decreases with the size reduction of the gold core. The melting temperature of AuNPs range between 300-400°C while it is 1064°C in the bulk state [51]. In nanoscale, melting starts at the nanocrystal surface, and decreases the total surface of energy. Due to this fact, a large reduction in temperature is attributed to the distinct contribution of surface atoms to the free energy of the system, which favors the solid-liquid transition. Optical and conductive behavior of nanoparticles is also size-dependent due to the variation of the electronic energy levels density where the wave functions of charge carriers are spatially confined [52]. Using the Fermi level of metal nanoparticles to those of bulk metal and

molecular clusters in comparing the electronic structure and band occupancy, the quantum effects changes as a function of the dimension of the nanocrystal interior. The valence electrons of a bulk piece of metals occupy energy bands instead of discrete energy levels. Valence and conduction bands consist of molecular orbitals which are separated by the Fermi level and are infinite in number, the highest occupied energy level at absolute zero. There is no energy gap separating the valence band from the conducting band in a metallic conductor, thus electrons are promoted to the conduction level by thermal energy. As the object size decreases to the nanoscale, the edges of the band become discrete energy levels.

Therefore, in metals, where the Fermi energy level is situated at the center of the band, the spacing between energies is still very small. Hence, the energy band appear as a continuum of energy states. Therefore, the quantum confinement effect of metallic nanoparticles is expected to occur only at quite small size because otherwise, their electronic properties resemble those of bulk metal.

2.4.2. Optical properties of metallic nanoparticles

The large ratio of nanoparticles' surface area to their volume depicts their outstanding optical properties. This feature makes the optical properties of nanoparticles different from their usual bulk ones. For instance, the familiar yellowish color attributed to gold is exhibited by the bulk format [53,54]. However, its color tends to be different step-by-step until it becomes ruby red by subdividing it into nano-size scale. The absorption spectra of colloidal solutions of AuNPs with dimensions less than the incident wavelength have unique colors and is characterized by a broad and intense peak in the visible region of the spectra. The spectral measurements of AuNPs colloidal solution reveal that their ruby red color is due to their absorption of the green light at 520 nm [55].

In this regard, Beer's law helps to calculate the solution's absorption (A). Using the spectrophotometer, the attenuation in the intensity of the incident light (I_0) is measured, which happens when the light with (I) intensity passes through a colloidal solution with a concentration of (C), molar absorptivity of ε, and with an optical path length of b [56]. The rate $\frac{I_0}{I}$ is the attenuation rate (that is, the loss of photon), and is given by:

$$A = \varepsilon bC \qquad\qquad (1)$$

$$A = log\frac{I_0}{I} \qquad\qquad (2)$$

The absorption (A) is a quantity without unit since both I_0 and I have the same unit. By changing the particle size and shape as well as the dielectric function of the surrounding environment as stated previously, the peak position, height, shape, and bandwidth of AuNPs spectra could be tuned [57].

2.4.3. Surface Plasmon Resonance

Stable metallic nanoparticles; for example, gold and silver nanoparticles (NPs), react with the incident light strongly. Due to the excitation of surface plasmon in such particles, the particle plasmon or localized surface plasmon resonance (LSPR) are created. The excited plasmon in metal nanoparticles (MNPs) is localized to the particle and not characterized by a wave vector, even though normal light cannot excite plasmon in a planar metal as the momentum of both surface plasmon (SP) and photon must be matched. As a result, with no need for any geometry for momentum coupling, the incident light is absorbed. For such LSPR, the absorbed light has to have a specific wavelength called a plasmon band [58].

11

Fig. 1 diagrammatically depicts the creation of surface plasmon resonance in a spherical MNP on applying an electromagnetic (EM) field. The electric field (E) induces polarization in the conduction electrons with respect to the heavier positive core. The conduction electrons oscillate under the influence of the applied field based on the assumption that the positive charges are immobile. The electronic cloud gets displaced from the positive ionic core as a consequence of the coherent oscillations of the conduction electrons, giving a chance to a net charge difference at the nanoparticle boundaries, which results in a coulombic attraction and a linear restoring force that leads to the dipolar oscillations of the electronic cloud with respect to the positive ionic core. The described oscillation is known as surface plasmon resonance or oscillation. The term "surface" comes from the idea that the restoring force that causes the resonance comes from the surface polarization. Therefore, the surface of the MNPs plays a significant role in observing the LSPR [58,59]. When the frequency of the electric field of the incident light resonates with the oscillation of the free conduction electrons of MNPs, then the localized mode of SP occurs. Therefore, a large enhancement up to a factor of 100 is produced in the local electric field in close proximity due to the illuminated MNPs which are excited and strongly absorb/scatter the incident light [36]. The enhancement in the local field is given by the sum of the incident electric field and the one that is induced by SP in MNPs [61].
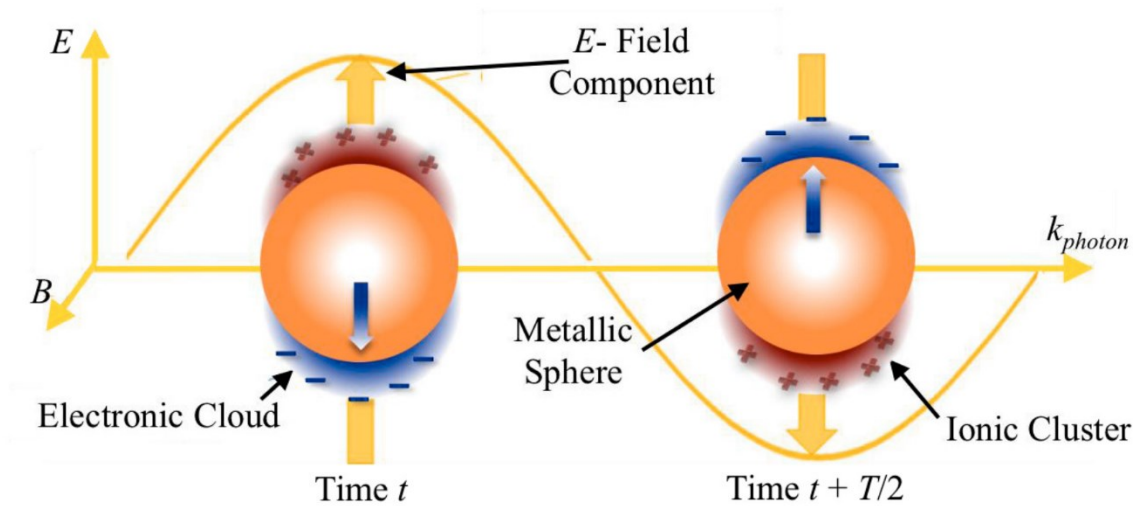
Fig. 1 Exposure of an EM field (i.e. light) with nanoparticles such as gold which creates SPR

(adopted from Refs. [57,58]*).*

The LSPR excitation mode is supported by a wide range of metallic nanostructures/particles. Metallic nanoparticles are easily synthesized using wet-chemical synthesis process and are usually kept stable in colloidal solutions. They can have any shapes; e.g. spheres, discs, rods, stars, cubes, rings, etc. As shown in Fig. 2 The colloidal solutions of MNPs exhibit fascinating colors due to their interaction with the incident light, since their resonance condition occur in optical frequencies [62]. In terms of synthesis, AuNPs could be synthesized in a reproducible manner with a uniform diameter by the reduction of the Au using sodium citrate. This method produces AuNPs that are stable in solution and negatively charged. In addition, adjusting the concentration of the reagent controls the size of the particles. Yet, AuNPs could be aggregated by the addition of more salt or evaporating the solvent. In contrast, aggregation is prevented by synthesizing NPs using capping ligands which stabilizes them. The capping makes the size-tuning possible and produces anisotropic particles [60].
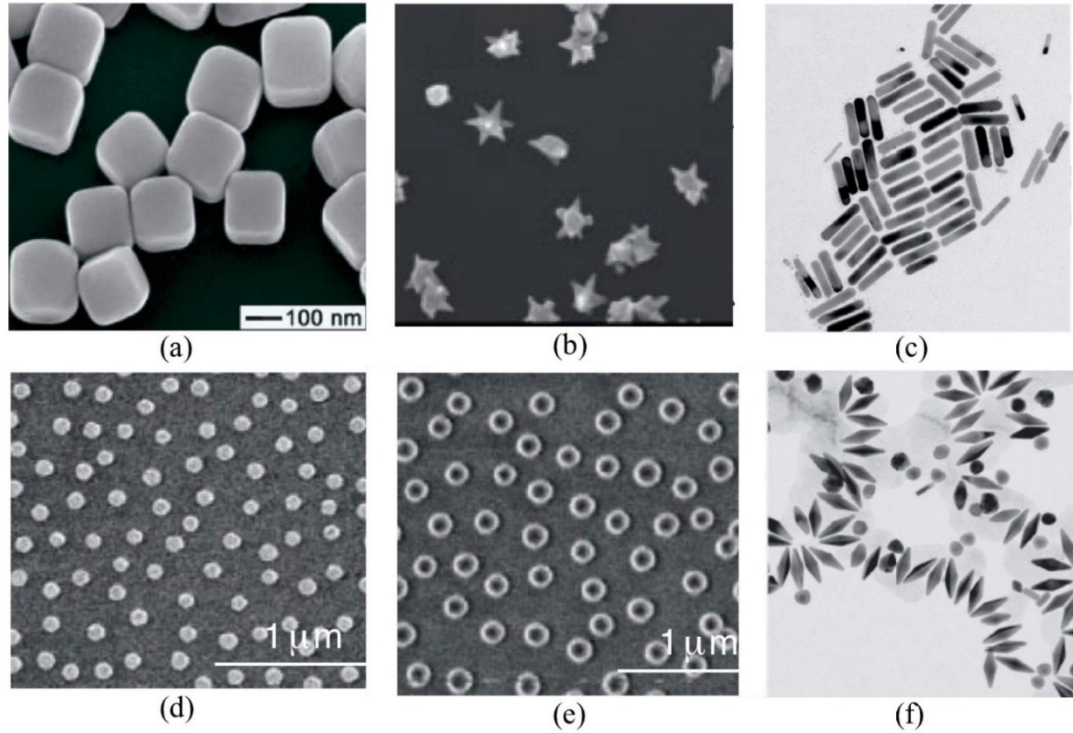
Fig. 2 Morphology of MNPs : (a) Silver nanocubes (b) Gold nanostars (c) gold nanorod (d) gold nanodiscs (e) gold nanorings; and (f) gold nanobipyramids (adopted from Ref. [60]).

2.4.4. Anisotropic effect

The optical properties of AuNPs are noticeably related to the morphology and geometry of the nanoparticles. For instance, when nanospheres are completely symmetrical, there is only one dipolar plasmon resonance. However, nanorods AuNPs present a second dipolar resonance band in the longitudinal direction is possibly formed. For more complicated geometries, the optical absorption becomes more complex due to the more non-degenerated dipolar modes increase. Also, higher multipolar charge distributions exist in less symmetrical particles. The locations of the higher multipolar surface plasmon resonances are always at the longer wavelengths with respect to the dipolar ones (red-shifted). Fig. 3 shows the relationship of the AgNPs shape and extinction efficiency [63].

14
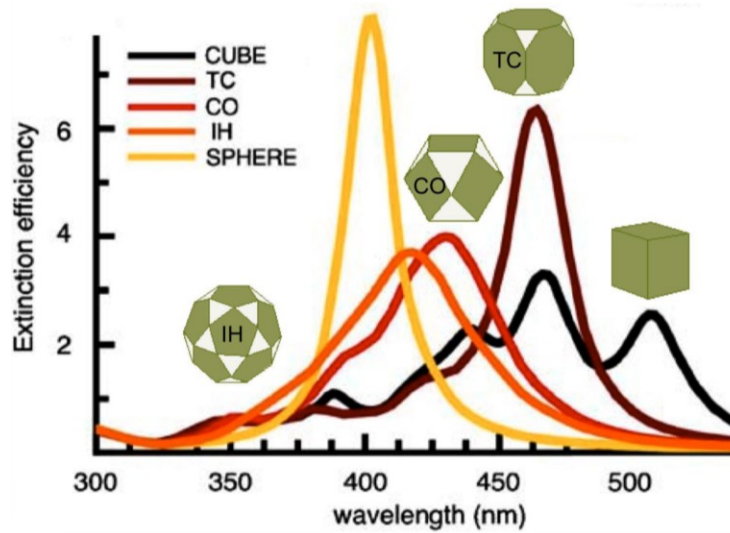
Fig. 3 Extinction efficiency of silver nanoparticles with various shapes (adopted from Refs. [63]*).*

2.4.5. Size effect

When we zoom in nano-sized scale, the ratio of NPs radius to the incident wavelength becomes important, and the optical features become size-dependent. For fine particles (< 10 nm) the diameter of the particles becomes comparable or less than the mean free path of the electron. This results in electrons collisions with the surface of the nanoparticles. Hence, the electrons' effective mean free path reduces linearly in comparison with bulk materials. Hence, the metal-dielectric characteristics vary from the dielectric function in the bulk form of material. This affects the plasmon resonance band to be broadened as shown in Fig. 4 [59,64].
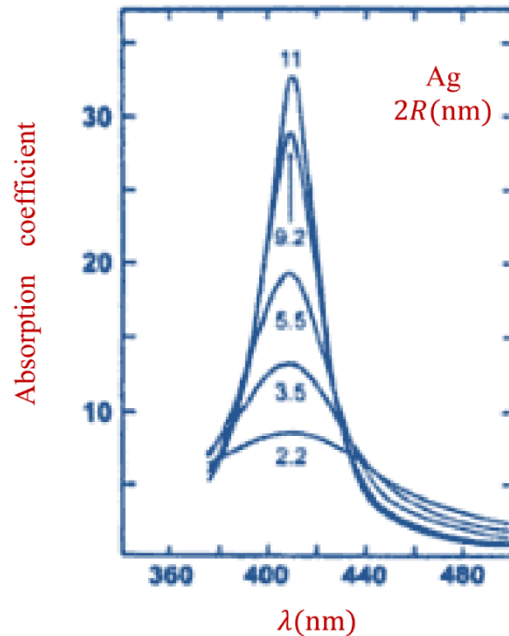
Fig. 4 Size confinement effects on the plasmon resonance band for Ag nanoparticles (adopted

from Refs. [64]*).*

For NPs with diameter less than 30 nm, the excitation of the conduction electrons occurs in-phase with the incident EM radiation, which results in a dipolar oscillation. Therefore, the scattering becomes insignificant and the absorption will be the dominant contributor to the extinction cross section.

Increasing the nanoparticles' size (>100 nm), resulting in raising the absorption and scattering becomes dominant. Furthermore, light cannot polarize large particles homogeneously. In addition, the peaks appear broadened, redshifted, and less intense. As the size of the particles grow bigger, a split in the energy levels is reduced until they merge into the quasi-continuous band structure for bulk solid. Fig. 5 presents the extinction properties of spherical AuNPs in water as a function of diameter. AuNPs utilize in many optical applications,

including sensors and PV devices due to its feature in scattering and absorbing incident light [59,64].
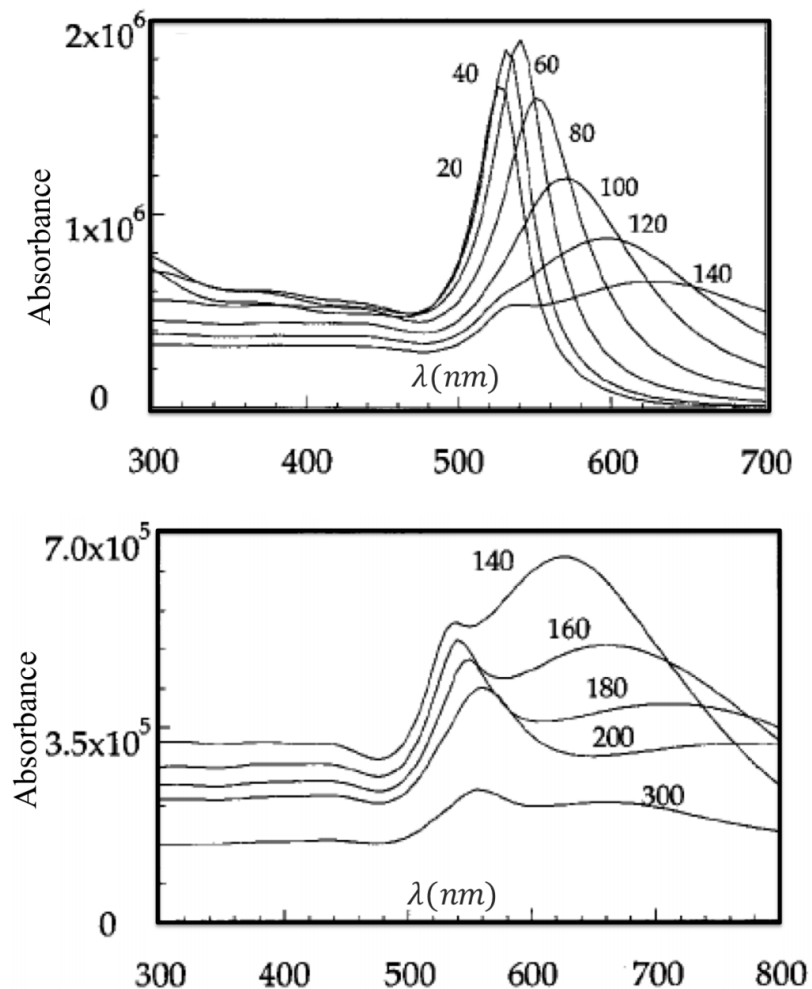
Fig. 5 Absorption bands of gold nanoparticles in water as a function of diameter. By increasing the particles' size, various extinction peaks appear, and then peaks fade away (adopted from Refs. [65]).

2.5. Methods of synthesis

In the previous decade, many scholars have developed different methods for AuNPs synthesis. Based on the recent studies by selecting optimum experimental conditions and suitable ligands, nanoparticle size and polydispersity is controllable. Proper ligand is vital for the particle

formation since it is related to ligand's ability to attach with newly formed nanoparticles without interfering with the metal ion reduction procedure. The ligand type in AuNPs synthesis is related to the stability of this material's suspension. Citrate reduction, amine stabilized nanoparticles, thiol stabilized nanoparticles, DMAP-stabilized nanoparticles are the most used methods for AuNPs synthesis that will describe bellow.

2.5.1. Citrate reduction

More than 50 years ago, Turkevich developed the most common and classical method for AuNPs reduction method, citrate reduction, which creates monodispersed water-soluble particles. This method is simple, quick and green with only three starting chemicals which do not need bulky equipment. In citrate reduction gold extracted from the $HAuCl_4$ structure and citrate act as a stabilizing group. The stability of AuNPs suspension is due to the assembly of citrate ions, having different oxidation states, at the gold nanoparticle's surface. Therefore, citrate which contains three carboxylic acid groups slightly neutralize the positive charge of the partially reduced Au atoms at the particle's surface and confer a strong negative charge that stops aggregating. In this process, the pH, and citrate concentrations is a vital variable that changes the geometry and size of the particles. Moreover, citrate itself is a weak acid that regulates the gold environment's pH.

These citrate-capped nanoparticles can be used due to the unstable property of the protective group in post-synthesis ligand modification, where the poorly defined surface functionality of the nanoparticle is provided specific functionalities. However, the nanoparticles have restricted stability for the same lability purpose as previously described, because they are very sensitive to pH and the existence of other organic materials [66,67].

2.5.2. Thiol stabilized nanoparticles

Brust [68] reported the direct synthesis of thiol-stabilized AuNPs in 1994 and successfully prepared dodecanethiol-capped gold nanoparticles. In this method, $HAuCl_4$ dissolved in water and moved to an organic environment (toluene) via a phase transfer agent, usually tetraoctylammonium bromide (TOAB). In this environment gold is reduced in the presence of alkyl thiol chains. The biphasic reaction gives very fine (1-3 nm) nanoparticles of which are sterically stabilized by the alkylated part of the ligand which thiol group covalently bound to the AuNPs surface. This stabilizes the suspension that also exists in a solvent-free form that can be later re-dispersed in a suitable solvent. Also, it is demonstrated that replacing the original toluene with methanol or THF, could form nanoparticles in a single-phase reaction, thus eliminating the use of phase transfer agents. Moreover, incorporation of water-soluble functionalities has let the design of single-phase synthesis, which allows the use of novel ligands, solvents and reaction conditions [67,69].

2.5.3. Amine-stabilized nanoparticles

Even though amine moieties have more weak affinities to gold, they can effectively balance out AuNPs in suspension. Leff et al. [70] reported amine-capped nanocrystals by simply substituting the thiol function of the Brust ligands for an amine. Other amino ligands, including amino acid lysine and other multifunctional amines, such as polymers, have also been used to form water-soluble suspensions. Similarly, to the citrate, primary amines are also used as reducing agents as they can nucleate and grow particles. These types of ligands are particularly attractive in biological and environmental systems as they are water-soluble and usually biocompatible. However, the nanoparticles synthesized with this method are generally bidder and their stability is more sensitive to pH variations [71,72].

2.5.4. DMAP-stabilized nanoparticles

Gittins and Caruso [73] worked on a simple one-step procedure to produce 4-6 nm-sized NPs, in order to change AuNPs from an organic to an aqueous media, which relies on the ability of 4-dimethylaminopyridine (DMAP in Fig. 6) to promote nanoparticle transfer into the polar phase. First, AuNPs form in toluene by means of a reducing agent and are temporarily protected by the labile ligand TOAB. The nanoparticles are then moved into the polar phase via the exchange of their weakly stabilized shell by the water-soluble DMAP ligand, which has a higher affinity to gold. Because of the phase separation of DMAP between water and toluene, a large excess of DMAP is required to fully displace the former ligand. The excess DMAP also plays a role in the NPs stabilization since the kinetically labile DMAP is in constant equilibrium between its bound and free form. Several studies suggest that the binding of DMAP to gold occurs through the lone doublet of the endocyclic nitrogen of the molecule that adopts a vertical position at the metal surface and that the nanoparticle stabilization is electrostatic as the exocyclic nitrogen of the resonant form of DMAP induces a positive charge at the gold surface [73,74].
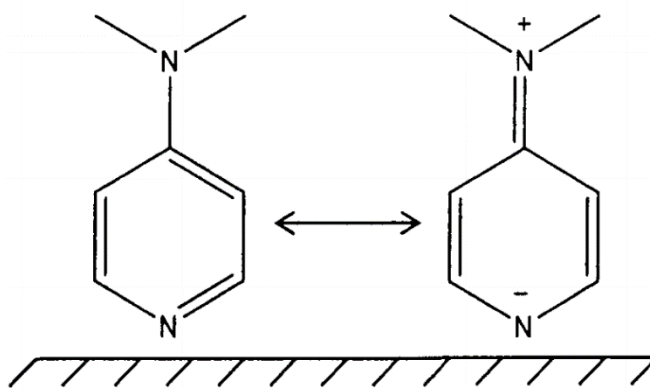
Fig. 6 structural representation of the two resonance forms of DMAP [75]

This means that DMAP does not adsorb onto AuNPs when the nitrogen at the binding site is protonated. Therefore, potentially, the stabilization of NPs is unlikely to occur below the pKa of DMAP, which is around 9.6. DMAP, however, remains associated with gold since the pH stability range goes well beyond DMAP's pKa. It was stated that the bound DMAP has a separate dissociation constant that exists only between pH 4.5 and 5, explaining the NPs' broad degree of pH stability. However, the nanoparticles are no longer soluble and precipitate below pH 5 in the solution. A very important feature often exploited in ligand-exchange reactions is the pH lability of DMAP molecules. [73,74].

2.6. Water pollution

Water is the most important solvent due to its different special properties; hence, it easily gets polluted. Water is considered as polluted when its quality and composition changes either naturally or as a result of human activities. Hence, making it less desirable for drinking, domestic, agricultural, industrial, recreational, wildlife usage. Water pollutant can be categorized into three main groups: physical, chemical or biological, leading to water's compositional change or aesthetic degradation which is ultimately detrimental for aquatic life and human consumption. However, a big chunk of the water pollutants are chemicals which remain dissolved or suspended in water and give an environmental objectionable response. Some most important physical pollutants are heat and radiations which have marked effects on organisms. Any factor can be recognized as a pollutant only in special circumstances, for instance, phosphorus is very important in the manure for growth of organisms, but the presence of its excessive quantities in water bodies leads to the problem of eutrophication [76–78]. Therefore, various examples of chemical pollutants including heavy metals [79], pesticides [80], and fertilizers [81,82]. In this section mercury,

cadmium, lead, uranium, nitrate and phosphate are discussed, which are good examples of heavy metals and fertilizer pollutants.

2.6.1. Mercury

Mercury is considered the third most hazardous element by the US Government Agency for Toxic Substances and Disease Registry (ATSDR) and is a neurotoxin that has severe harmful effects on human health and aquatic life. Three different types of mercury exist, called the elemental, organic, and inorganic mercury. Elemental mercury is used in thermometers and electrical switches in its pristine form. Some elemental mercury evaporates at room temperature and subsequently affects the lungs and kidneys. Methylmercury, which is organic mercury, is the most toxic form of mercury that gets into the human body through the eating of contaminated fish and seafood and is known to affect the brain and lead to behavioral abnormalities in infants. Inorganic mercury, for example, Hg^{2+} is the most stable form of mercury that gets into the environment by human activities and remains in the environment for a long time. Hg^{2+} damages the stomach, intestines, and leads to severe skin rashes. Mercury pollution occurs naturally through volcanic eruptions, evaporation from water bodies, and the Earth's crust. [83,84].

2.6.2. Cadmium

Cadmium can be found in phosphate fertilizers and cigarettes and is presently utilized in many processes such as electroplating or metallurgy. These various usage leads to an elevated cadmium exposure in the environment which is typified by the report of the increasing cadmium content in food. There have been many records on the harmful effects of Cd^{2+} on the bones, kidneys, nerve system, and soft tissues, with negative outcomes including renal dysfunction, calcium metabolism disorders, and an increased incidence of certain forms of cancers [85,86].

2.6.3. Lead

Lead is a highly toxic metal causing human and animal health disorders. Pipe network used in household plumbing is a primary source of contamination of drinking water with lead. In the last few decades, 50% of the lead emission originates from petrol. Recently it has been decreased due to the introduction of unleaded petrol. Moreover, food can get contaminated with lead during growing or processing, and packing. Low-level lead exposure is known to beget several health side effects. For instance, lead could cause delayed mental maturity in infants, and kidney daisies and high blood pressure in adults. Lead poisoning in human lead to severe damage to the liver, reproductive system, nervous system kidney and brain which leads to illness or death. Lead's severe exposure has been associated with abortion, stillbirth, sterility, and neonatal deaths. Also, studies show that long-term low-level lead exposure in children may diminished intellectual capacity [58].

2.6.4. Uranium

Uranium is regulated in drinking water by the United States Environmental Protection Agency (EPA) and classified as a radionuclide. 30 µg/L is the EPA's maximum contaminant level for uranium (MCL) in drinking water. However, prolonged exposure of elevated levels of uranium in drinking can result in kidney damage and is also connected to a higher risk of cancer. Uranium is speedily removed from the bloodstream and subsequently deposited in both the kidneys and skeletal bones. The skeleton is the main site of uranium accumulation in the human body. Reverse osmosis is a treatment technology for uranium removal from drinking water [87,88].

2.6.5. Potassium

Potassium is among the essential ions required to maintain body homeostasis. Moreover, to the importance of potassium in biological applications, it is also a crucial ingredient in soil quality assessment, coal combustion and flue gas cleaning systems and chemical laboratories. In certain polar drug compounds, the assessment of potassium is part of the study required for the release of the drug material for use in clinical supplies. The amount of potassium in the body must be controlled over a certain concentration range. Normal concentrations of potassium in the human body are between 3.5 and 5.9 mM in serum, 40–120 mM in urine, 5–10 mM in sweat and about 30 mM in saliva. Kidney excretion balances the intake of K^+. Kidney malfunction, neuromuscular issues, cell deaths, and the effect of some medications could change the urinary potassium. Moreover, for those patients who have spent a long time in the intensive care unit (ICU) or those who have had severe prolonged diarrhea and vomiting, there is a need to give them a special dosage of potassium [89].

2.6.6. Nitrate

Contamination of ground water with nitrate typically occurs from two sources; human/animal waste or synthetic fertilizers. Ammonia in human/animal waste is converted to nitrite (NO_2^-) by nitrifying soil bacteria in the nitrogen cycle:

$$NH_3 + 1.5O_2 \rightarrow NO_2^- + H^+ + H_2O \qquad (3)$$
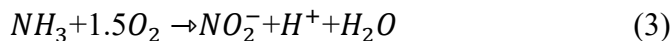
Nitrite is afterwards converted to nitrate (NO_3^-) by nitrifying bacteria in the soil which is an aerobic environment:

$$NO_2^- + 0.5\,O_2 \rightarrow NO_3^- \qquad (4)$$

Nitrate contamination of drinking water is a treat due to the medical condition called methemoglobinemia in the blood, which is also called "Blue Baby Syndrome". This is a dangerous condition that can cause death in kids below three months of age but can affect children up to eight years of age. Since micro-bacterial flora in their digestive tract of babies is not completely developed, they are noted as the most vulnerable to nitrate contamination. Methemoglobinemia occurs when nitrates oxidize ferrous iron (Fe^{2+}); therefore, altering the ferrous iron to ferric iron (Fe^{3+}) in the blood, which does not allow oxygen to bind to red blood cells. Mild effects of methemoglobinemia can instigate shortness of breath caused by an insufficient supply of oxygen to the blood. Blue lips on infants are a hint of more severe cases and can lead to asphyxiation and death [90,91].

2.6.7. Phosphorus

Phosphorus is one of the most necessary elements needed by all organisms. All living organism need phosphorus for (Adenosine triphosphate) ATP and (Adenosine diphosphate) ADP synthesis, which are essential for energy transfer processes. Also, phosphorus is used for the synthesis of DNA and RNA in plants. Phosphorus is a major constituent of cell membranes, and it is present in high concentrations in human and animals' teeth, bones, and shells. Although a huge amount of phosphorus is in the soil in forms that are unavailable for plants. Moreover, phosphorus fertilizer is needed to ensure plant productivity in many agricultural systems. Phosphate in the soil mainly exists as HPO_4^{2-} and $H_2PO_4^{-}$ ions, which are derived from weathering rock phosphate and from skeletal remains of animals and sea creatures. The phosphorous ions in the soil depend on the soil's pH. Acidic soils contain $H_2PO_4^{-}$ and when soil pH is greater than 7, phosphorus is in HPO_4^{2-} form. The HPO_4^{2-} and $H_2PO_4^{-}$ are equally present when pH is between 6 and 8. Moreover, Eqs. 5-6 present the transformation phosphate types in the nature (Fig. 7).

$$H_3PO_4 \leftrightharpoons H^+ + H_2PO_4^- \qquad\qquad pK_a = 2.17 \qquad (5)$$

$$H_2PO_4^- \leftrightharpoons H^+ + HPO_4^{2-} \qquad\qquad pK_a = 7.31 \qquad (6)$$

$$HPO_4^{2-} \leftrightharpoons H^+ + PO_4^{3-} \qquad\qquad pK_a = 12.36 \qquad (7)$$

| H₃PO₄ | H₂PO₄⁻ | HPO₄²⁻ | PO₄³⁻ |

H_3PO_4 Phosphoric acid — $H_2PO_4^-$ Dihydrogen phosphate — HPO_4^{2-} Hydrogen phosphate — PO_4^{3-} Phosphate
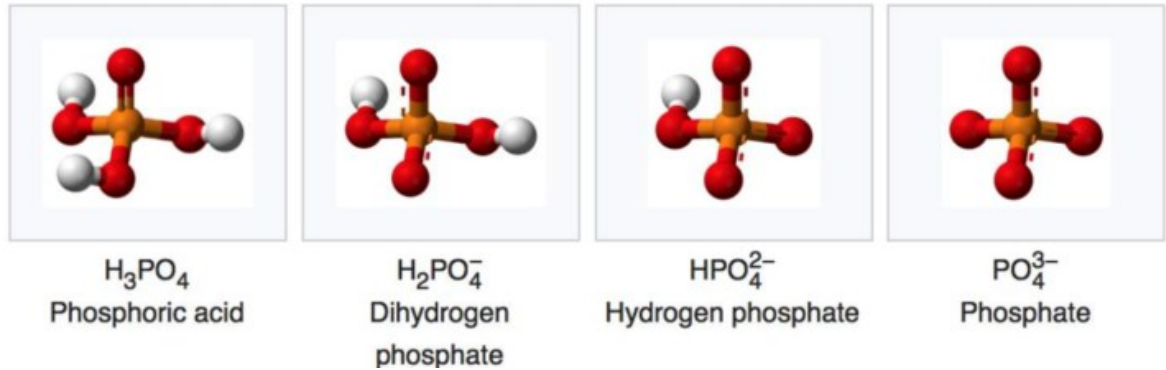
Fig. 7 Existing forms of phosphate ions in nature (adopted from Refs. [87]).

Water-soluble ions such as calcium and potassium move through the soil by diffusion and bulk flow, but phosphorus moves only through diffusion. The rate of diffusion of phosphorus is low (10^{-12} to 10^{-15} m²/s), and high uptake rates from a zone that is depleted of phosphorus around the roots of the plants. The availability of phosphorus in the soil is also affected by time and the more phosphorus passes through the soil the more time is needed for reactions to occur. Hence, the phosphorus cycle is the slowest biochemical cycle as the rock weathers phosphorus bearing minerals slowly. Insoluble phosphate minerals are the ultimate source of phosphorus for plants and animals, which is present as insoluble calcium phosphate named apatite ($Ca_{10}(PO_4)_6(OH, Cl, F)_2$ and it can be fulfilled by eating plants. Some phosphate ions are tightly bound to elements such as iron, calcium, and aluminum in compounds that are not very soluble in water. One of the important sources of phosphorus for plants is through recycling (Fig. 8) of phosphorus from

decomposing organisms. After the death of plants or organisms, organic phosphorus is converted to inorganic phosphorus by microorganisms.
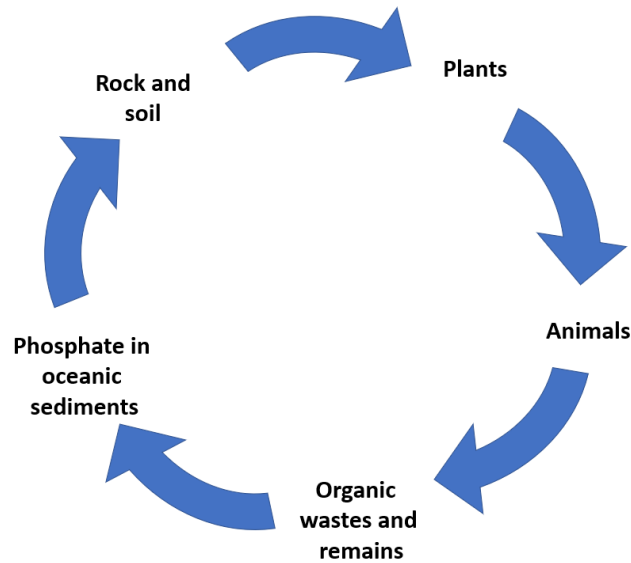
Fig. 8 Schematic diagram of phosphorus cycle

2.7. Introduction to eutrophication

Eutrophication is the process of increased enrichment of water bodies with nitrogen and phosphorus (especially in the format of phosphate) that stimulates excessive plant growth. For the growth of aquatic plants, phosphorus and nitrogen are needed. There is usually a shortage of these elements in natural bodies of water, thus keeping the spread of vegetation under control. When algae die, they sink to the bottom of the lake and are decomposed by bacteria. Large quantities of dissolved oxygen are used in the decomposition of algae and releases carbon dioxide. This causes a reduction in the amount of oxygen available for the aquatic organisms and fish, therefore limiting the growth of the aquatic population and often causing the death of fish. Eutrophication is one of the significant environmental challenges observed in inland waters. Eutrophication results in sediment build up at the bottom of the lake from eroded soil particles. The water storage capacity

of the lakes is decreased by the sediment build up. Phosphate concentration exceeding 0.05 mg/L and nitrate concentration about 10 mg/L lead to eutrophication. The natural process of eutrophication takes several hundred to thousands of years, but eutrophication can be greatly increased by human activities [92–94].

Lakes classification is an important topic in the eutrophication investigation. Based on the degree of enrichment of lakes with nutrients, lakes are categorized into four different types (Fig. 9). Oligotrophic lakes, mesotrophic lakes, eutrophic lakes, and dystrophic lakes. Oligotrophic lakes are freshwater lakes that have a low supply of plant nutrients. Oligotrophic lakes are poor habitat for fishes due to the shortage of food for aquatic life consumption. The phosphorus concentration in oligotrophic lakes is reported to be approximately 0.008 mg/L. Biological productivity of oligotrophic lakes is very low and usually consider as a source for drinking water because of low algae production [93,94].

Mesotrophic lakes are moderately supplied with plant nutrients which are greater than oligotrophic lakes and consider as a transitional state between oligotrophic and eutrophic. During the summer season, mesotrophic lakes behave differently compared to oligotrophic lakes by separating into layers. The top layer becomes hot during summer and supports little algae growth [93,94].

Eutrophic lakes have high levels of biological productivity due to increased concentration of nitrogen and phosphorus. The phosphorus concentration in eutrophic lakes is reported to be approximately 0.05 mg/L. These excess plant nutrients support massive plant growth which leads to heavy growth of phytoplankton or rooted aquatic plants, the water becomes turbid and cannot

be used as the drinking water. Deep waters in eutrophic lakes have reduced concentrations of dissolved oxygen [93,94].

Dystrophic lakes are highly polluted and support massive algae growth. These lakes contain dark colored water and are low in pH. The dark color is caused by organic acids, mainly humic acid, from the surrounding due to the decomposition of plant residues. The organic solutes producing coloring in oligotrophic and eutrophic systems are generated within the system by the decomposition of plant remains (autochthonous). The acidic conditions and lack of oxygen in the deep layers of the dystrophic lakes cause the death of fish [93,94].
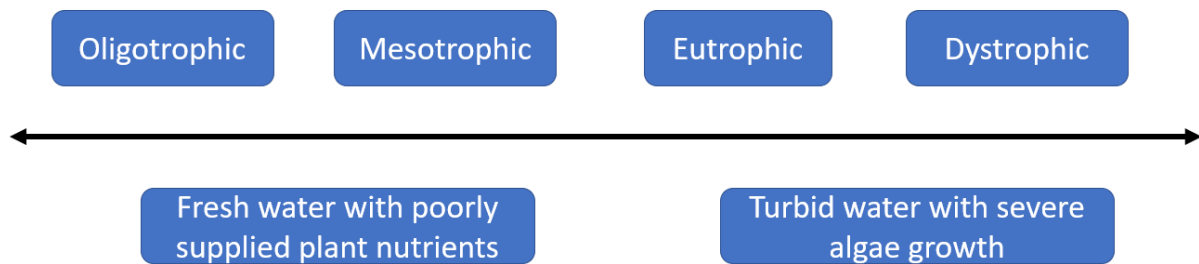
Fig. 9 Trophic classification of lakes(adopted from Refs. [94]).

Based on the conducted research, the phosphate is a vital element, but the excess amount of this material could cause severe problems. The current methods for detection of phosphate are expensive, bulky, energy storage needed, and operator needed. To sum up, the aim of this project is to fabricate an easy to use, inexpensive and sensitive sensor for phosphate detection.

Chapter 3. Experimental Procedures

This chapter's focus is on the experimental steps carried out on this research project and explains the gold and tablet fabrications in detail.

3.1. Materials and methods

Gold (III) chloride solution 99.99% (trace metals basis, 30 wt. % in dilute HCl) and trisodium citrate dihydrate were purchased from Sigma Aldrich, Canada. Mercaptoacetic acid 97% (MA), europium (III) nitrate hexahydrate 99.99%, and sodium phosphate 0.5 M buffer solution (pH 7) were purchased from Fisher Scientific, Canada. HPLC grade water, hydrochloric acid (HCl), nitric acid (HNO₃) and tris were obtained from the Fisher Scientific, Canada. Lithium sulfate 98.5%, potassium sulfate 99%, manganese (II) sulfate monohydrate 98%, iron (III) nitrate nonahydrate 98%, ammonium sulfate 99%, nickel (II) nitrate hexahydrate, zinc nitrate hexahydrate, cobalt (II) nitrate hexahydrate 99%, sodium sulfate, aluminum oxide, calcium chloride dihydrate and dextran were purchased from Sigma Aldrich, Canada. The pullulan was purchased from Polysciences, USA. All reagents were used as received and not further purified. The filter paper Whatman #1, #2 and #4 were purchased from Fisher Scientific, Canada.

For the synthesis of gold nanoparticle, the experimental setup presented in Fig. 10 was used, which consist of a triple-neck round bottom flask and a condenser purchased from Concordia University central store, Montreal, Canada. Sartorius analytical weight balance was used for measuring chemicals weight. Isotherm hot plate stirrer was utilized for boiling and mixing the solutions purchased from Fisher Scientific, Canada. Moreover, monitoring the pH was also important in all the experiment stages which conducted with MQuant paper-based pH indicator

30

and AB200 pH/mV/conductivity indicator, both purchased from Fisher Scientific, Canada. The Thermo Fisher scientific spectrophotometer Evolution 2020 device was used for evaluating the solution's color absorption and iPhone Xs used for taking the pictures. Moreover, transmission electron microscope (TEM) (FEI Titan Krios Cryo-STEM (working at 200 kV)) was employed for structural examinations and investigation of particles morphology and size. Malvern Zetasizer Nano ZS also used for zeta potential calculation. The real sample phosphate detection was also conducted by Metrohm 930 Compact IC Flex.
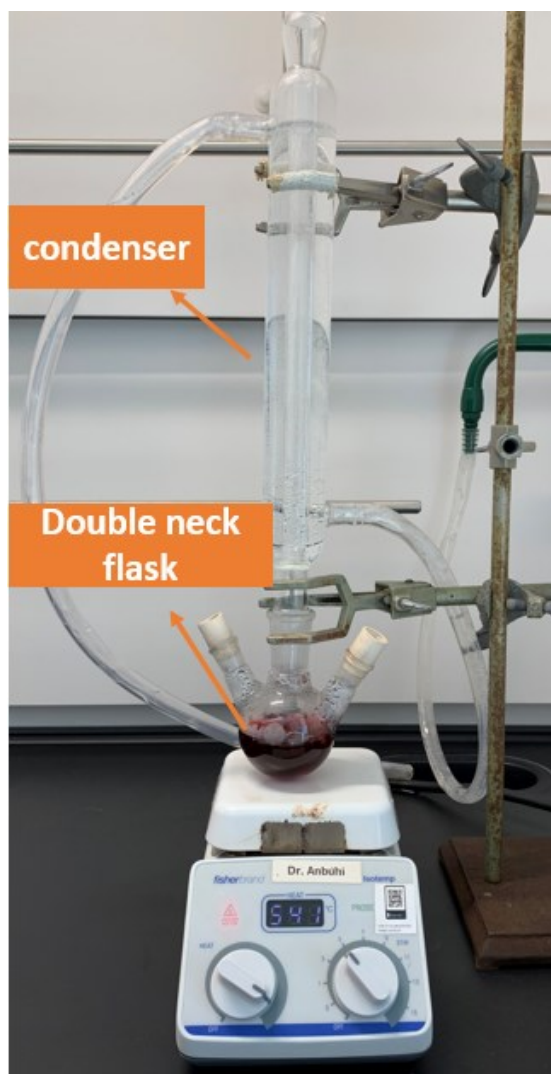
Fig. 10 The setup for synthesis of gold nanoparticle.

31

3.2. Preparation of mercaptoacetic acid-capped gold nanoparticles (MA-AuNPs)

All glassware and magnetic stir bars in the synthesis were thoroughly cleaned with freshly prepared aqua regia (HCl: HNO_3 3:1, v/v), rinsed with double distilled water, and air-dried to avoid premature nucleation during the synthesis, as well as aggregation of the gold colloid.

The citrate-capped AuNPs were synthesized by the classical Turkevich reduction method as described in the literature [95] and Fig. 12 illustrates the step-by-step procedure for the MA-AuNPs preparation. 45 mL of 1.0 mmol. L^{-1} $HAuCl_4$ solution was boiled with vigorous stirring in a 100 mL three-neck round-bottom flask equipped with a condenser to maintain a constant volume of the reaction mixture. At the boiling point, 5 mL of 38.8 mmol. L^{-1} trisodium citrate (Fig. 11 A), causing a rapid color change from faint yellow to wine-red (Fig. 13), indicating the formation of AuNPs. The mixture was heated under reflux for an additional 30 min at boiling temperature and afterwards stored at 4 °C [18].
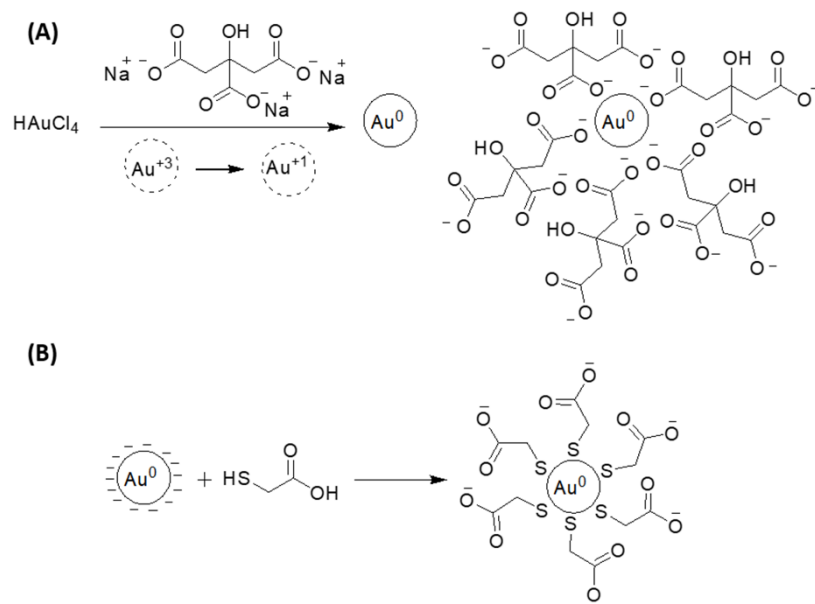
Fig. 11 Steps for synthesis and functionalization of AuNPs (A) reduction and stabilization with citrate ions, (B) functionalization with mercaptoacetic acid.

After the synthesis, the AuNPs solution was diluted twice with HPLC grade water. In the next step, the AuNPs were functionalized with mercaptoacetic acid, (Fig. 12 D and Fig. 11 B). 125 μL of 14 mM mercaptoacetic acid was added to 40 mL of the synthesized gold suspension, and the resulting mixture was stirred for 2 h at room temperature to get.

Afterwards, the suspension was centrifuged (10,000 rpm, 30 min), followed by the decantation of the supernatants to remove the excess of MA. In this section, the synthesized gold nanoparticle was divided into four parts, of which 3 are adjusted with tris-HCl buffer, ammonia-buffer and tris-buffer respectively, and the last is left in its pristine state.
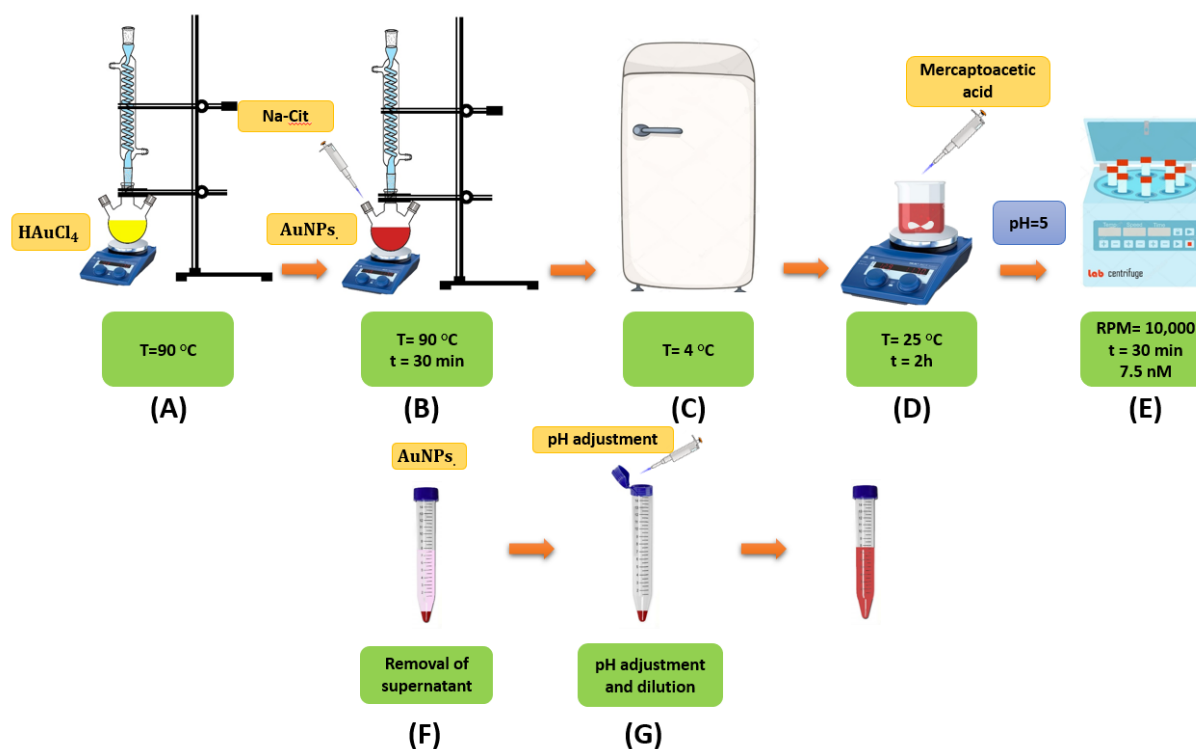
Fig. 12 Procedure for the preparation of functionalized mercaptoacetic acid-capped gold nanoparticles (MA-AuNPs). (A) Synthesis of the AuNPs starts with boiling HAuCl₄ followed by (B) addition of sodium citrate (Na-Cit) as a reducing agent. After the synthesis, (C) the AuNPs are stored in the fridge at 4 °C. (D) To functionalize the AuNPs, MA is added to the solution and stirred for 2h. (E) The solution is centrifuged to remove the excess MA. (F) The supernatant, which is the desired MA-AuNPs product, was separated from the distillate. (G) Addition of HPLC water to the solution and adjustment of pH with tris-buffer HCl, ammonia-buffer and tris-buffer.
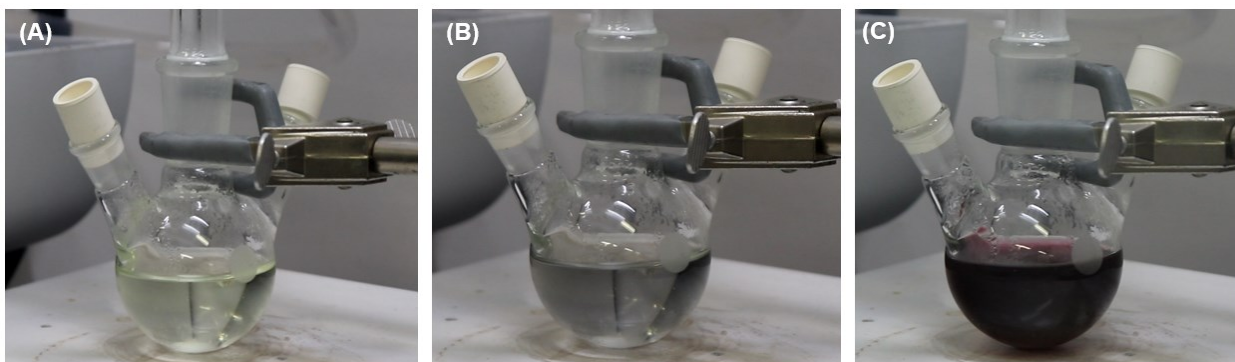
Fig. 13 The solution color change in the Turkevich method (a) the is yellow at the first stage (boiling gold solution). (b) After addition of the sodium citrate (Na-Cit), the color turns gray and then (c) after boiling for 10 minutes the wine-red color appears.

3.3. Europium and gold tablet preparation with dextran and pullulan

The 7 % and 10 % dextran/pullulan tablets were prepared by mixing 0.14 mg/0.2 mg of dextran/pullulan powder with 2 mL solution of 220 µM Eu^{3+} solution. Afterwards, 75 µL of the resulting solution were dropped using a micropipette on a plastic sheet and allowed to air dry to form the Eu^{3+}- dextran/pullulan tablets. The tablet preparation was done in ambient air and at room conditions. The tablets were then left to dry for 24 h. The 7 % AuNPs tablet was prepared with the same procedure as described above, 0.14 mg of dextran/pullulan powder mixed with 2 mL solution of AuNPs solution. Afterwards, 375 µL of the resulting solution was dropped on a plastic sheet using a micropipette and allowed to air dry to form the AuNPs-dextran solid tablets.

Chapter 4. Results and Discussion

In this chapter the results of the fabricated sensor in the two formats of tablet and paper are discussed. This include the optimization of Eu^{+3} concentration; first, the europium optimized in two environments with pH 7.4 and pH 5.8. The optimized concentration with the best pH is selected for the calibration curve preparation and tablet fabrication. Selectivity, stability and interfering studies of the developed sensor are presented as well.

4.1. Characterization

The appearance of wine-red color confirmed the formation of AuNPs and the surface

plasmon resonance (SPR) wavelength absorbance of citrate capped AuNPs emerged at 520 nm

(Fig. 14).
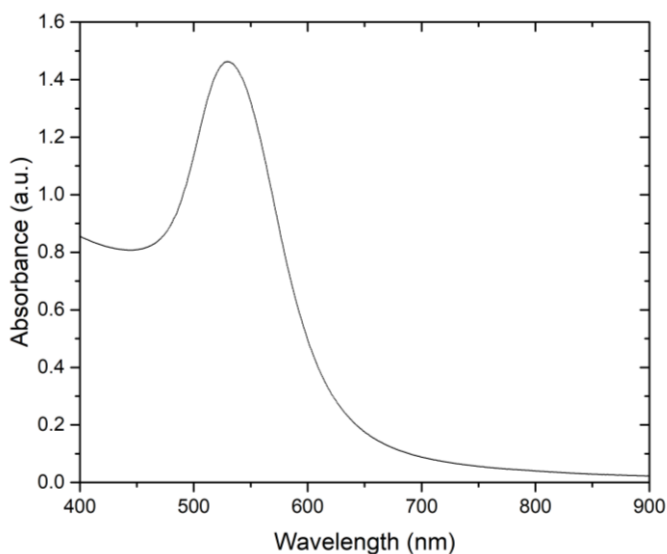
Fig. 14 UV-Vis graph after gold nanoparticle synthesis by the Turkevich method.

Based on the transmission electron microscopy (TEM) in Fig. 15, synthesized AuNPs'

average diameter of the particles calculated with Digimizer Image Analysis Software and it was

12.9 ± 0.8 nm with a polydisperse format.
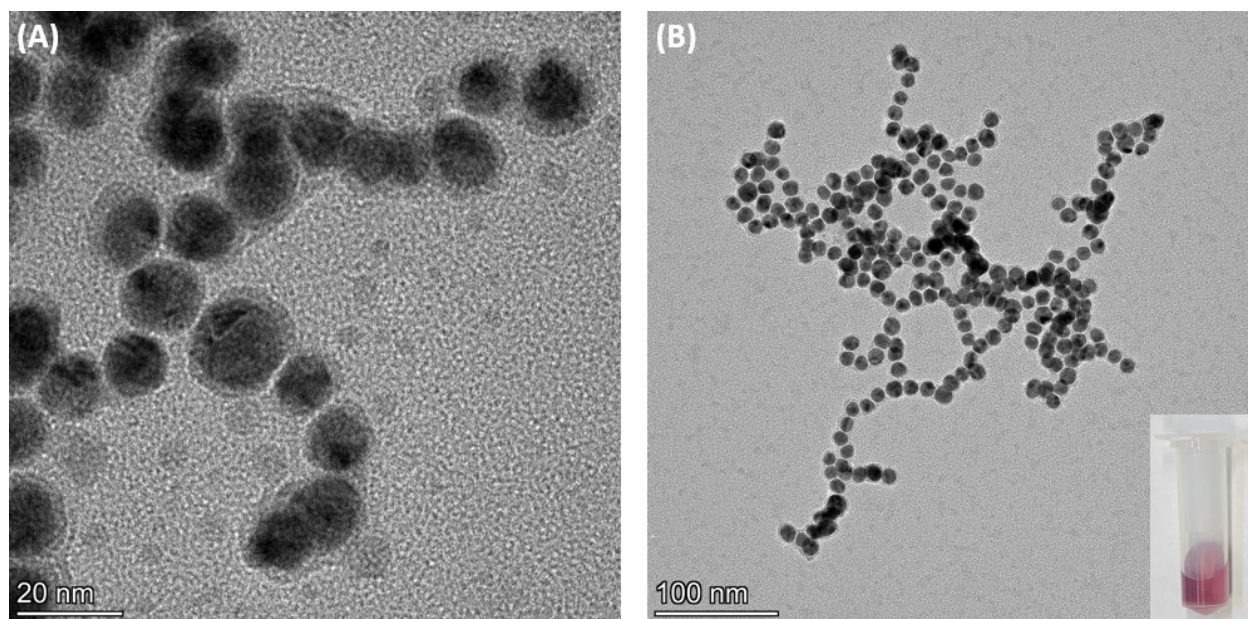
Fig. 15 TEM image of synthesized gold nanoparticles (the red solution on the bottom right corner is an image of the AuNP solution)

For the functionalization step, MA-AuNPs were formed by the ligand exchange reaction between citrate capped AuNPs and MA due to strong Au-S bonding. The attachment/interaction of mercaptoacetic acid's thiol group with AuNPs is covalent while the other end of the ligand remains free. This available carboxylate end of the molecule interacts with Eu^{3+}, hence promoting chelation reaction [16].

4.2. Optimization of Eu^{3+} concentration with a pH adjusted MA-AuNPs solution (pH 7.4)

Based on the stoichiometric reaction between the Eu^{3+} and the phosphate ions (Eu (III) + $PO_4^{-3} \rightarrow EuPO_4$), the detection of the phosphate concentration in solution is related to the Eu^{3+} concentration in the same solution. Due to this relationship, Eu^{3+} concentration was first optimized to determine the required concentration which can cause a sharp color output. In this regard, various concentrations of Eu^{3+} (*i.e.*, 150 to 400 μM) were tested with MA-AuNPs (pH adjusted to 7.4 using tris-buffer HCl) to find the optimum color change of wine-red to blue. Based on the

ImageJ analysis in Fig. 16 (A), color transition from red to purple happened at the 200 μM of Eu^{3+} and turned to blue and no further color change was observed by increasing the Eu^{3+} concentration higher than 230 μM. So, Eu^{3+} concentration of 230 μM was selected for the assay development.

The color change kinetic of MA-AuNPs by addition of 230 μM of Eu^{3+} solution was monitored by the absorption ratio of Red/Blue intensity, as shown in Fig. 16 B. Due to the fast aggregation of the MA-AuNPs, the absorption ratio is sharp. The rapid crosslinking process of MA-AuNPs by Eu^{3+} is due to carboxylate groups on the MA-AuNPs surface and hence the rapid crosslinking of MA-AuNPs would be induced. The obtained results showed that the MA-AuNPs aggregation process triggered by Eu^{3+} was completed within ~ 6 sec.
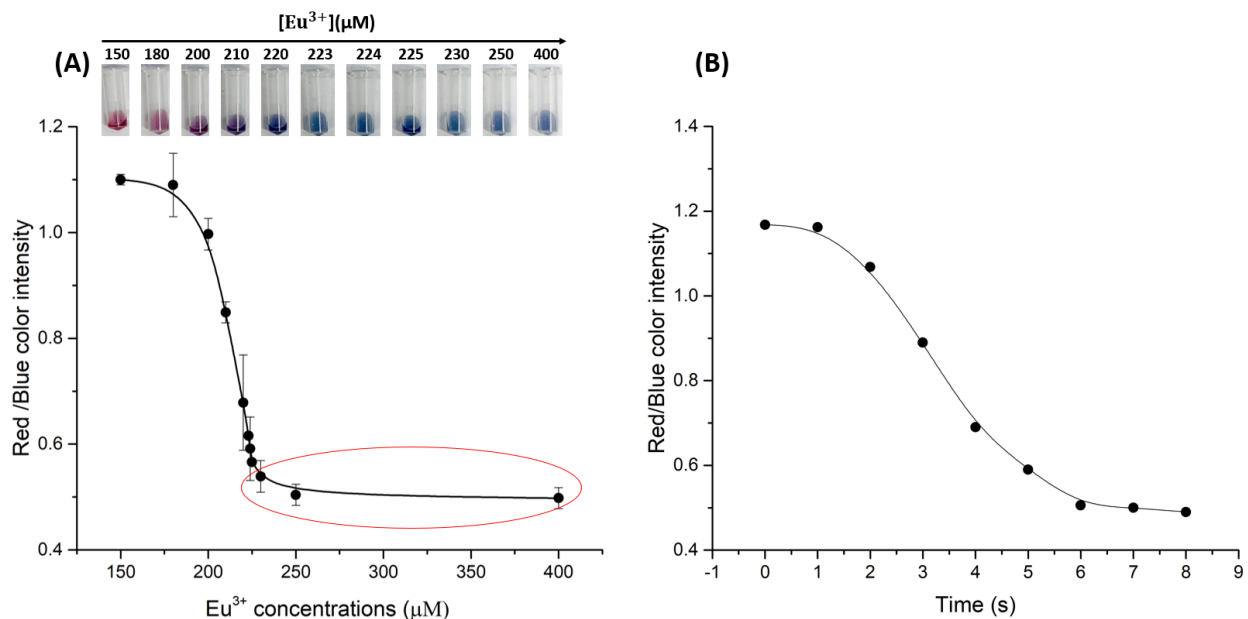
Fig. 16 (A) Calibration of Eu^{3+} concentration; at concentrations of 150, 180, 200, 210, 220, 223, 224, 225, 230, 250, and 400 μM, along with the Red/Blue ratio of samples obtained by ImageJ (B) Kinetic of MA-AuNPs aggregation with 230 μM of Eu^{3+} solution.

4.3. Colorimetric phosphate detection with a pH adjusted AuNPs solution (pH 7.4)

For the colorimetric detection of phosphate, the optimized concentration of Eu^{3+} (230 µM) solution was premixed with a series of phosphate solutions (0.5 to 200 µM) and incubated for 10 min. After addition of MA-AuNPs (pH adjusted to 7.4 using tris-buffer HCl), with the increase of Pi concentration from 0 to 200 µM, the solution color changed from blue to purple, and finally to red, which indicated the transition from the aggregation state to dispersion state of AuNPs (Fig. 17).
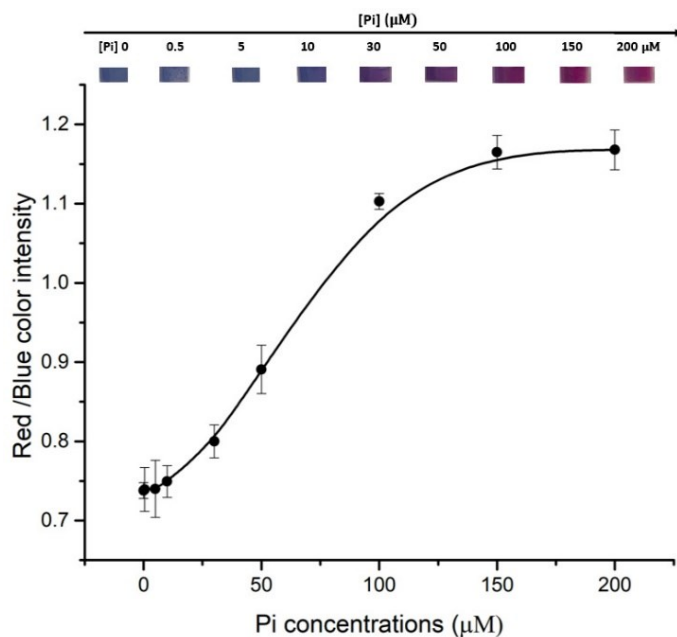
Fig. 17 Colorimetric detection of Pi, at concentrations of 0.5, 5, 10, 30, 50, 100, 150 and 200 µM along with the Red/Blue ratio of samples obtained by ImageJ .

By increasing the concentration of Pi, the Red/Blue ratio also increased. Firstly, the color of MA-AuNPs which mixed with Pi concentration of 0.5 and 5 µM, remained blue, since the Pi molecules were not enough to deactivate the aggregation. With increasing Pi concentration

38

(between 10 and 30 µM), the Eu^{3+} aggregation effect is gradually deactivated, and the solution color turned to bluish-purple. Further increasing of Pi concentration led to color change to reddish-purple (between 50 and 100 µM) and finally wine-red (between 150 and 200 µM). This obviously demonstrated that Pi works as an anti-aggregation agent through interrupting the coordination of the surface-bound carboxylate groups on AuNPs with Eu^{3+}. Also, the calculated lower and upper limit of detection of the assay gotten from the formula LOD = Xb1 +/- 3Sb1, where Xb1 is the mean concentration of the lowest/highest signal and Sb1 is the standard deviation of the lowest/highest signal [44]. The lower limit of detection was found to be as low as 22.10 µM, and the upper limit of detection was found to be as high as 111.12 µM.

The pH adjustment was also conducted with ammonia-buffer (pH 11) and solution of tris-buffer (pH 10.4). However, ammonia-buffer was unsuccessful in adjusting the pH and tris-buffer had similar effects as the tris-HCl buffer (Fig. 18). Based on the stability test which is also presented in the Fig. 22 (B), the MA-AuNPs sample contain tris-buffer HCL was only stable for 3 hours. Moreover, the ζ-potential of the sample which contained tris-buffer HCl (pH of 7.4) was -8.53±1.35 mV which shows the instability of the colloid.
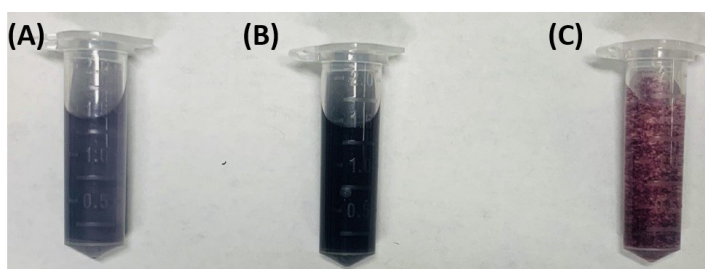
Fig. 18 Stability of MA-AuNPs solution with tailored pH using (A) tris-buffer HCl, (B) tris-buffer, (C) ammonia-buffer after 3 hours.

4.4. Optimization of Eu^{3+} concentration without a pH adjusted MA-AuNPs solution (pH 5.8)

Regarding Eu^{3+} optimization with MA-AuNPs solution which its pH has not been adjusted with buffer (pH is 5.8), concentrations of Eu^{3+} (160 - 226 μM) were tested to find the optimum value based on the color change of red to blue. As shown in Fig. 20 (A), the obvious color transition from red to purple happened at the 200 μM of Eu^{3+} and turned to blue further increasing the concentration up to 220 μM. No further color change was observed by increasing the Eu^{3+} concentration beyond 220 μM since the red/blue color remained constant. The TEM image in Fig. 19 also confirms that this concentration of Eu^{3+} can completely agglomerate the MA-AuNPs. Hence, 220 μM of Eu^{3+} was chosen as the optimum concentration for the Eu^{3+} tablets fabrication.
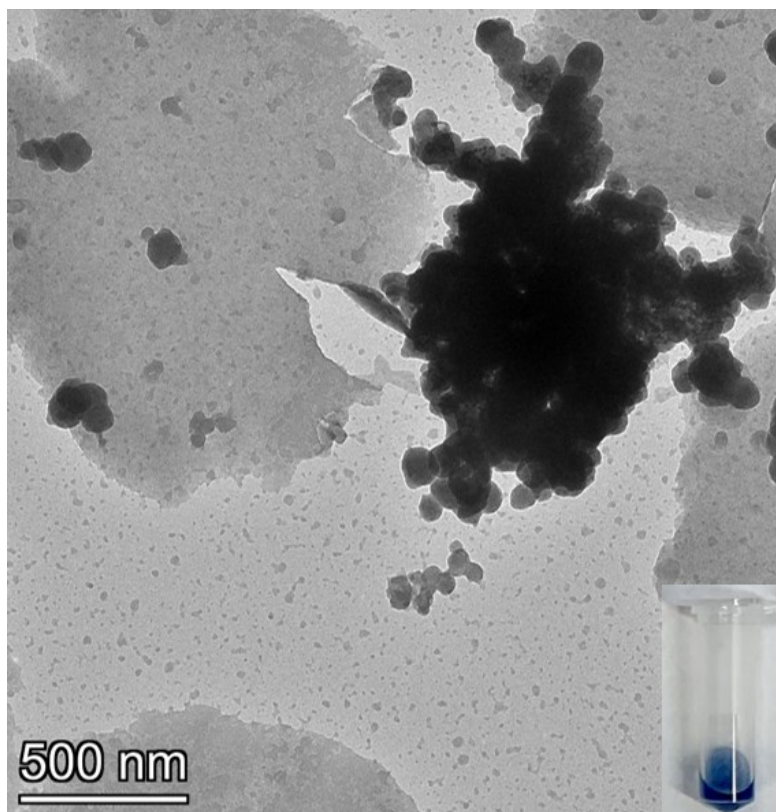
Fig. 19 TEM image of agglomerated functionalized gold nanoparticles with 220 μM Eu^{3+} (the blue solution on the bottom right corner is an image of the MA-AuNP solution)

Furthermore, the aggregation kinetic of MA-AuNPs containing 220 μM Eu^{3+} has been quantified by monitoring the red/blue color change in intensity over time (Fig. 20 (B)). As the kinetic graph reveals, the red/blue color intensity decreased sharply to its minimum within only 35 seconds. This data highlights that this optimum concentration of Eu^{3+} gives us assay results in a time as low as 35 seconds, which is unprecedented.
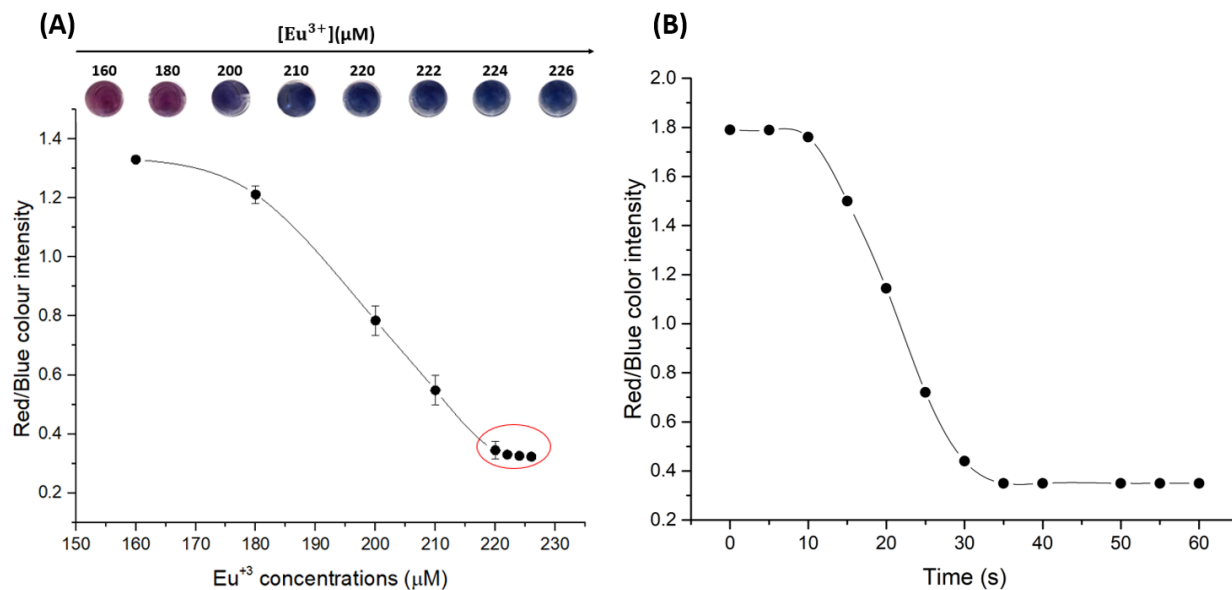
Fig. 20 (A) Optimization of the concentration of europium ion to be used in the assay for effective sharp color change from red to blue using europium concentration from 0 to 226 μM. (B) The aggregation kinetic of 220 μM europium ion in functionalized gold nanoparticles (MA-AuNPs).

4.5. Colorimetric phosphate detection without a pH adjusted AuNPs solution

After the determination of the optimum concentration of Eu^{3+} (220 μM) needed for an effective color output due to the aggregation of the gold nanoparticles, the Eu^{3+} solution was transformed to tablets and a calibration curve for the quantification of the amount of phosphate in water was investigated. At this point, the final solution in the microtubes will either turn blue or red based on the concentration of phosphate in the solution. The color intensity of the final solutions was then computed using the Image J software and used to generate a quantification

41

curve. As shown in Fig. 21, there were color outputs of blue and red in the microtubes and the red/blue color intensity of the final solution increased as the amount of phosphate ion present in the solution increased. This showed that the amount of phosphate in water can be quantified by the color intensity of the red to blue ratio of the assay. Furthermore, the concentration of phosphate in water can be detected to a value as low as 0.0625 µM (by the naked-eye detection of color change) which gives a better sensitivity when compared to the work of Wenquan Liu et al. [39]. Also, the lower and the upper limit of detection of the assay were calculated using the formula LOD = Xb1 +/- 3Sb1, where Xb1 is the mean concentration of the lowest/highest signal and Sb1 is the standard deviation of the lowest/highest signal [44]. The lower limit of detection was found to be as low as 0.0315 µM (3.779 µg/L), and the upper limit of detection was found to be as high as 2.7369 µM (0.328 mg/L). The detection of phosphate in the water at this wide detection range confirms that MA-AuNPs are very sensitive and an excellent sensor upon which basing the quantification of phosphate in solution.

The MA-AuNPs solution without the tris-HCl buffer was found to be stable for at least 3 weeks which is due to the electrostatic feature of the colloidal solution of the AuNPs (the stability tests were stopped due to lockdown caused by the Covid-19 pandemic) (Fig. 22(A) and Fig. 23).

(A) Without Tris-HCl Buffer

(B) With Tris-HCl Buffer
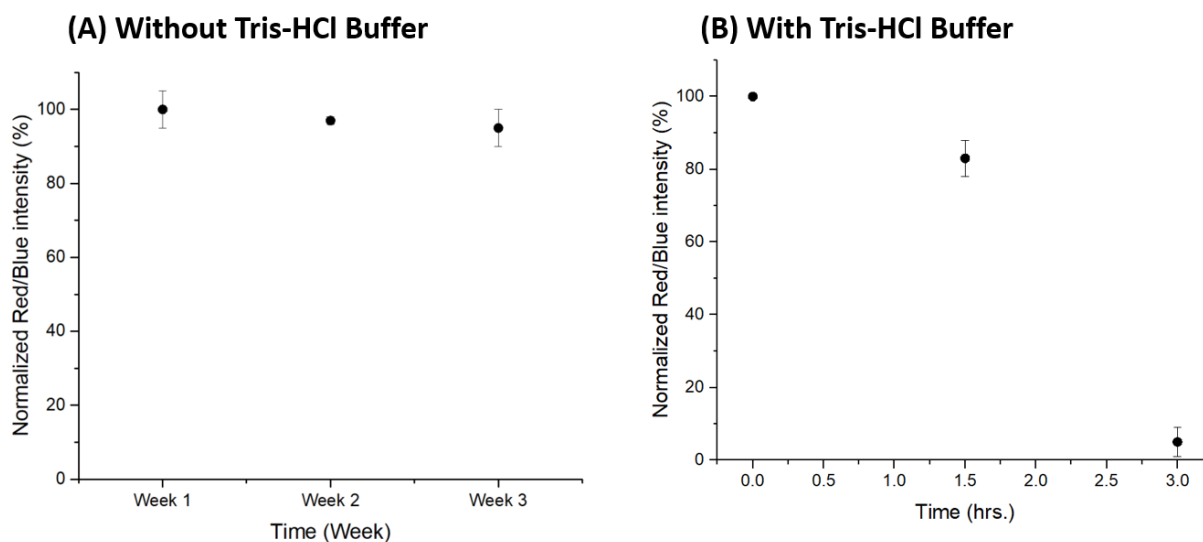
Fig. 22 Stability test on the MA-AuNPs for the detection of phosphate for (A) up to 3 weeks at room temperature at pH 5.8 (without any buffer) and (B) for 3 hours at room temperature at pH 7.4 (with tris-HCl buffer).
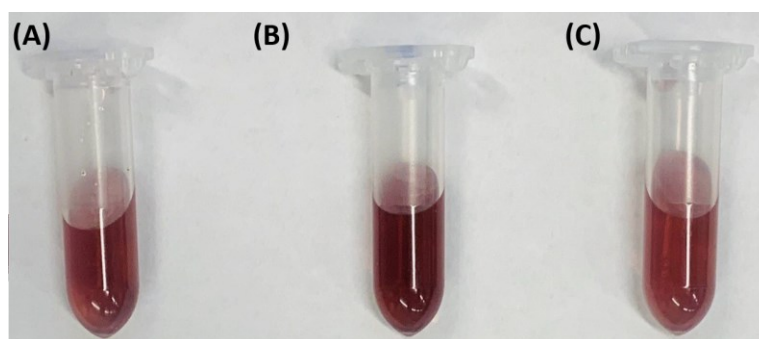
Fig. 23 Stability of the MA-AuNPs solution without tris-buffer HCl for (A) week 1, (B) week 2 and (B) week 3.

Moreover, the zeta potential of both MA-AuNPs samples' were analyzed which provide valuable information about the charge carried by the nanoparticles and; hence, about the stability

43

and ability of the particles to react with analyte molecules. Based on the data acquired by Dynamic Light Scattering, the sample with the pH of 5.8, which does not have pH controller, has the ζ-potential of -28.93$\pm$0.41 mV. However, by addition of tris-HCl buffer, the solution was found to be very unstable and the ζ-potential of the MA-AuNPs changed to -8.53$\pm$1.35 mV. It is obvious that pH controllers disrupt the electrostatic balance of material and due to the higher absolute number of ζ-potential in MA-AuNPs with pH 5.8, this colloidal solution was more stable.

To sum-up, pH regulator, varying the limit of detection of Pi and ζ-potential of MA-AuNPs based on the conducted experiments. The MA-AuNPs with a pH of 7.4 using tris-buffer HCl is only stable up to 3 hours and detect 111.12 µM of phosphate in water. However, by removing tris-buffer HCl, the pH decreases to 5.8 and the sensor became stable for at least 3 weeks. In addition, the LOD of the sensor reduced to 2.7369 µM which is more sensitive in comparison with the assay with tris-buffer HCL. The results are summarized in Table 2.

Table 2 Summary of performance of AuNPs functionalized with or without tris-HCl buffer.

Assay type	pH	ζ-potential [mV]	Eu^{3+} [µM]	LOD [µM]		Stability
				Lower	Upper	
AuNPs with tris-buffer HCl	7.4	-8.53$\pm$1.35	230	22.10	111.12	3 hours
AuNPs without tris-buffer HCl	5.8	-28.93$\pm$0.41	220	0.0315	2.7369	3 weeks

4.6. Quantitative detection of phosphate using dextran tablet

After optimizing Eu^{3+} (220 µM) for the sharpest color output and change due to the aggregation of the MA-AuNPs (Fig. 24), a simple assay kit for the qualification and quantification of the phosphate amount in water was designed. Both pullulan and dextran tablets were tested for

their ability to release the MA-AuNPs and Eu^{3+} into solution. Results demonstrated that the dextran tablets worked better than pullulan tablet. Hence, the dextran tablets were selected to move forward. The structural formula illustration of the effect of the presence of europium ions and phosphate ions in the essay is shown in Fig. 25 A. This structurally illustrates the aggregation of MA-AuNPs due to the presence of europium ion (Fig. 25 A-I) and the disaggregation of MA-AuNPs due to the presence of phosphate ions (Fig. 25 A-II). The operational principle of the assay is then presented in Fig. 25 B, which qualitatively gives a "yes "or "no" output if the amount of phosphate in water is higher or lower than 0.0625 µM, respectively.
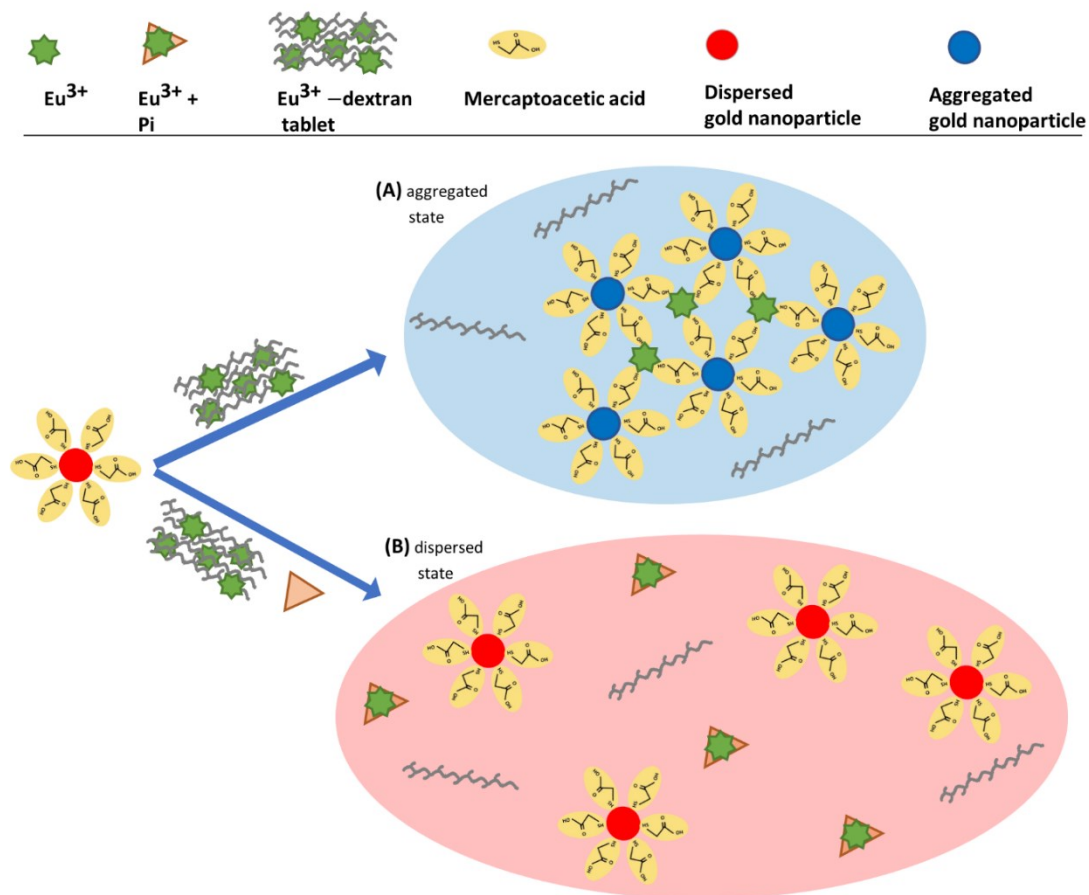
Fig. 24 The surface plasmon resonance property of gold nanoparticles, which makes them blue when in the aggregated state and red when in the dispersed state. (A) The europium ions invoke

aggregation of the nanoparticles, and (B) the presence of phosphate inhibits the effect of europium and causes a dispersion.

As illustrated in Fig. 25 B, the Eu^{3+}-dextran tablet is introduced into a microtube which is filled up with the water sample up to 500 µL. The complete dissolution of the tablet takes about 10 min. In the second step, the end user adds the aqueous solution of MA-AuNPs to the microtube and record the results after 35 seconds. If the solution color turns blue, it means that the water sample contains a phosphate concentration lower than 0.0625 µM. Otherwise, if the solution color turns purplish red, the water contains a phosphate concentration higher than 0.0625 µM because the phosphate molecules have re-disperse the MA-AuNPs complex.

This simple point-of-use assay required no special equipment or trained technician and the results are read with naked eyes and give a yes or no output. Also, for further quantification, the color intensity curve has been adopted in Fig. 21with the calculated lower limit of 0.0315 µM (3.779 µg/L), and the upper limit of 2.7369 µM (0.328 mg/L).
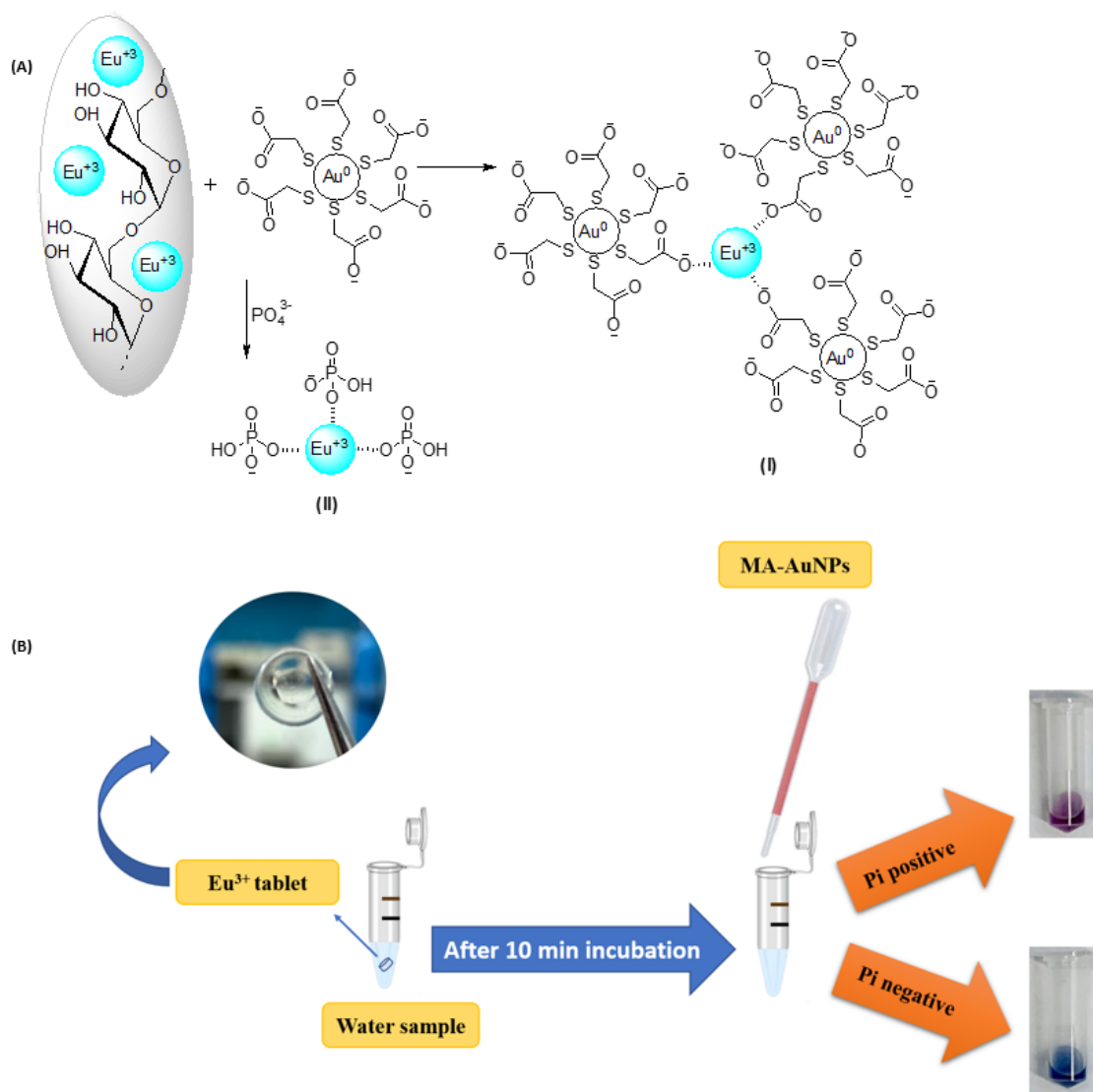
Fig. 25 Operational principle. (A) The behavior of europium towards: I. mercaptoacetic acid-gold nanoparticles (absence of phosphate) and II. phosphate. (B) Point-of-use operational principle of the device for the qualitative detection of phosphate in water.

4.7. Selectivity and recovery experiments of the developed Pi sensor

The selectivity of the sensor was evaluated by monitoring the red/blue color intensity response in the presence of other ions, including SO_4^{2--}, NO_3^-, Li^+, Ni^+, K^+, NH_4^+, Mn^{2+}, Zn^{2+}, Ni^{2+}, Co^{2+}, Fe^{3+}, Al^{3+} and Ca^{2+}. As shown in Fig. 26, 1 mM of these interference ions were

47

spiked into water and tested with the MA-AuNPs assay in comparison with the 0.25 µM phosphate solution. The insignificant color intensity ratio of red/blue was detected for these interference ions, even though their concentration was more than 300% higher than that of the phosphate ion solution. These results clearly reveal that the selected ions have no interference with the effectiveness and performance of the sensor.

The tablet-based sensor was used to determine phosphate concentration in real water samples with both low and high levels of phosphate concentrations, including water samples from Cote-des-Neiges in Montréal (tap water), Downtown Montreal (tap water), Saint Lawrence river in Montréal, and HPLC grade water. The concentration of phosphate determined with the tablet sensor for the HPLC grade water, the Cote-des-Neiges Montréal tap water, the Downtown Montréal tap water, and the Saint Lawrence river was 0 ± 0.001, 0.050 ± 0.001 (0.0059 ppm), 0.049 ± 0.001 (0.0058 ppm)and 1.021 ± 0.008 µM (0.1224 ppm), respectively. This was done by using the Image J software to compute the red/blue color intensity of the assay and comparing the values to the calibration curve. The red/blue color intensity of the HPLC grade water was 0.30, which depicts the absence of phosphate ions in the solution. The red/blue color intensity computed using the Image J software for was the Cote-des-Neiges Montréal tap water, the Downtown Montréal tap water, and the Saint Lawrence river was 0.40, 0.45 and 1.75 respectively. In order to validate the acquired data of the fabricated sensor, ion chromatography (IC) analysis was conducted on the real-water samples above. The phosphate level in the Saint Lawrence river was 0.175 ppm with the IC device, which is quite close to the concentration acquired by the fabricated sensor (0.1224 ppm). Due to the low concentration of Pi in the tap water samples and HPLC water, the IC system reported the phosphate limit as invalid.
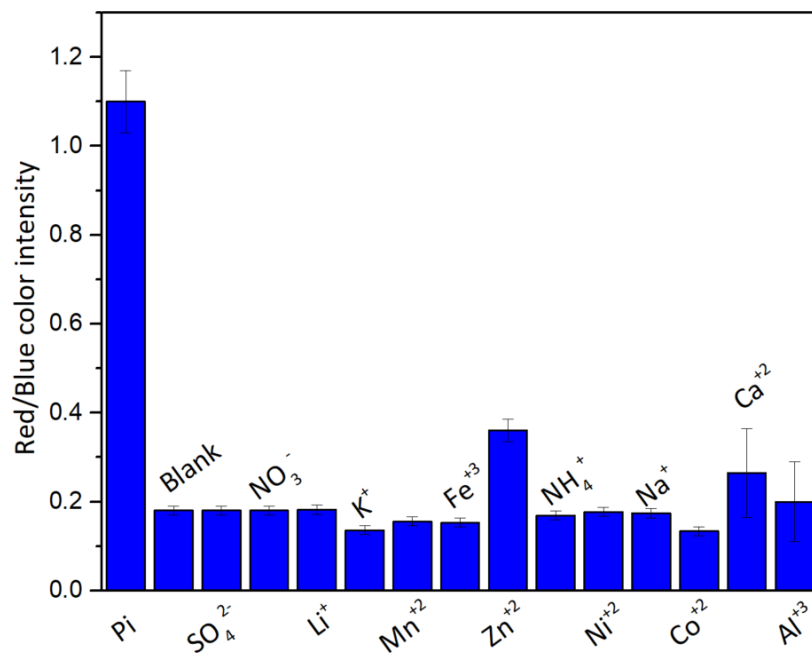
Fig. 26 Interference test of common ions present in water in comparison with that of phosphate ions. 0.25 μM of phosphate solution was compared with 1 mM of SO_4^{2-}, NO^{3-}, Li^+, K^+, Mn^{2+}, Fe^{3+}, Zn^{2+}, NH^{4+}, Ni^{2+}, Na^+, Co^{2+}, Al^{3+} and Ca^{2+} in water.

Chapter 5. Conclusions and Future Works

In section, the accomplished objectives briefly explained and sum-up this part with the future research topics.

5.1. Conclusions

This study's focus was on fabricating and optimizing an easy-to-use tablet-based sensor for phosphate ions detection in water. In the first step, spherical gold nanoparticles (AuNPs) were synthesized with the standard Turkevich reduction method. The light absorption properties and nanoparticles' morphology investigated by using UV-visible and transmission electron microscopy (TEM). The fabricated AuNPs were then functionalized with mercaptoacetic acid (MA) by exploiting carboxylate group which both inorganic phosphate (Pi) and Eu^{3+} show affinity and elicit the assembly/ disassembly of MA-AuNPs. Next, the effect of tris-buffer-HCl, tris-buffer and ammonia-buffer as pH controllers investigated and as the result, samples which did not contain pH controller revealed more sensitivity and stability.

Finally, the phosphate testing tube and Eu^{3+}-dextran tablet have been designed that are fast (response in 35 seconds), simple and represent a portable platform for the detection of phosphate in water. The sensor's principle is based on the color change enacted by the aggregation and dispersion of the AuNPs in the presence of Eu^{3+} and phosphate ion respectively. This method provides an inexpensive ($\simeq$ \$3 for 100 tests) means of determining the concentration of phosphate in water. The developed sensor is very sensitive with the calculated lower limit of detection of 0.0315 µM (3.779 µg/L) and upper limit of detection of 2.7369 µM (0.328 mg/L). Also, the sensor did not interfere with common ions present in the water and was stable for at least 3 weeks.

50

5.2. Future works

This research has contributed to fabricate an easy-to-use sensor with functionalized gold nanoparticles to detect phosphate in water. However, phosphate is not the only factor for the creation of eutrophication. Other components including nitrate can accelerate this phenomenon. Moreover, further investigations are required to obtain a more functional tablet-based sensor. Further research in this area can be extended in the following areas:

- The findings of this thesis are based on experimental observations. Mathematical models can therefore be produced and computed to promote rapid reproducibility and assay predictions.

- Based on the presented results in this thesis, the end-user should carry the functionalized gold solution in a tube for the test which is not much convenient. The further investigation could be on transforming gold nanoparticles in an easier to handle format such as tablet or paper-based platforms.

- As mentioned, there are some other components, including nitrate that impacts the creation of eutrophication. Further research could be conducted on detection of those elements based on the tablet-based devices and the design of a comprehensive detection kit for all chemicals that could cause eutrophication.

- Beside phosphate and nitrate, potassium plant fertilizer is extensively used in the farms. This potassium nutrient could cause severe side effects contaminating water resources. Therefore, the detection of potassium in water could be investigated using tablet-based platforms.

- More attention is required to explore the behavior of the temperature and pH towards sensitivity and stability of the MA-AuNPs sensor for phosphate detection using Eu^{3+}.

Chapter 6. References

[1]   Isachenko, A.I., Apyari, V. V., Melekhin, A.O., Garshev, A. V., Volkov, P.A., Dmitrienko, S.G., "Borohydride-modified polyurethane foam: a new form of a widely known reducing agent in synthesis of metal nanoparticles for sensing applications", *Applied Nanoscience*, Vol. 10, pp. 1023–1033, 2020.

[2]   Verma, M.L., Kumar, P., Sharma, S., Dhiman, K., Sharma, D., Verma, A., *Gold nanoparticle-mediated delivery of therapeutic enzymes for biomedical applications*, 2020.

[3]   Kalishwaralal, K., Luboshits, G., Firer, M.A., *Synthesis of gold nanoparticle: peptide–drug conjugates for targeted drug delivery*, 2020.

[4]   Yaman, Y.T., Vural, O.A., Bolat, G., Abaci, S., "One-pot synthesized gold nanoparticle-peptide nanotube modified disposable sensor for impedimetric recognition of miRNA 410", *Sensors and Actuators B: Chemical*, Vol. 320, pp. 128343, 2020.

[5]   Li, S., Pang, C., Ma, X., Li, H., Zhao, M., Liu, C., Luo, J., "A gold nanoparticle-loaded molecularly imprinted switch sensor with high sensitivity to ethephon", *Microchemical Journal*, Vol. 157, pp. 105025, 2020.

[6]   Sinha, A.K., Suzuki, K., Takahara, M., Azuma, H., Nonaka, T., Fukumoto, K., "Mesostructured manganese oxide/gold nanoparticle composites for extensive air purification", *Angewandte Chemie International Edition*, Vol. 46, pp. 2891–2894, 2007.

[7]   Babaei, Z., Rezaei, B., Pisheh, M.K., Afshar-Taromi, F., "In situ synthesis of gold/silver nanoparticles and polyaniline as buffer layer in polymer solar cells", *Materials Chemistry and Physics*, Vol. 248, pp. 122879, 2020.

[8]   Tran, Q.N., Lee, H.K., Kim, J.H., Park, S.J., "Influence of gold–silver rough-surface nanoparticles on plasmonic light scattering in organic solar cells", *Journal of Nanoscience and Nanotechnology*, Vol. 20, pp. 304–311, 2020.

[9]   Gancheva, T., Virgilio, N., "Tailored macroporous hydrogels with nanoparticles display enhanced and tunable catalytic activity", *ACS Applied Materials & Interfaces*, Vol. 10, pp. 21073–21078, 2018.

[10]   Heinze, K., "The quest for mononuclear gold(II) and its potential role in photocatalysis and drug action", *Angewandte Chemie International Edition*, Vol. 56, pp. 16126–16134, 2017.

[11]   Buffa, A., Mandler, D., "Arsenic(III) detection in water by flow-through carbon nanotube membrane decorated by gold nanoparticles", *Electrochimica Acta*, Vol. 318, pp. 496–503, 2019.

[12]   Tan, S.-Y., Lee, S.-C., Okazaki, T., Kuramitz, H., Abd-Rahman, F., "Detection of mercury (II) ions in water by polyelectrolyte–gold nanoparticles coated long period fiber grating sensor", *Optics Communications*, Vol. 419, pp. 18–24, 2018.

[13]   Guo, Y., Wang, Z., Qu, W., Shao, H., Jiang, X., "Colorimetric detection of mercury, lead and copper ions simultaneously using protein-functionalized gold nanoparticles", *Biosensors and Bioelectronics*, Vol. 26, pp. 4064–4069, 2011.

[14]   Daniel, W.L., Han, M.S., Lee, J.-S., Mirkin, C.A., "Colorimetric nitrite and nitrate detection with gold nanoparticle probes and kinetic end points", *Journal of the American Chemical Society*, Vol. 131, pp. 6362–6363, 2009.

[15]   Boken, J., Thatai, S., Khurana, P., Prasad, S., Kumar, D., "Highly selective visual monitoring of hazardous fluoride ion in aqueous media using thiobarbituric-capped gold nanoparticles", *Talanta*, Vol. 132, pp. 278–284, 2015.

[16]   Liu, W., Du, Z., Qian, Y., Li, F., "A specific colorimetric probe for phosphate detection based on anti-aggregation of gold nanoparticles", *Sensors and Actuators B: Chemical*, Vol. 176, pp. 927–931, 2013.

[17]   Oyewunmi, O.D., Safiabadi-Tali, S.H., Jahanshahi-Anbuhi, S., "Dual-modal assay kit for the qualitative and quantitative determination of the total water hardness using a permanent marker fabricated microfluidic paper-based analytical device", *Chemosensors*, Vol. 8, pp. 97, 2020.

[18]   Hormozi-Nezhad, M.R., Abbasi-Moayed, S., "A sensitive and selective colorimetric method for detection of copper ions based on anti-aggregation of unmodified gold nanoparticles", *Talanta*, Vol. 129, pp. 227–232, 2014.

[19]   Kannan, B., Jahanshahi-Anbuhi, S., Pelton, R.H., Li, Y., Filipe, C.D.M., Brennan, J.D., "Printed paper sensors for serum lactate dehydrogenase using pullulan-based inks to immobilize reagents", *Analytical Chemistry*, Vol. 87, pp. 9288–9293, 2015.

[20]   "Water: Monitoring & assessment", *https://archive.epa.gov/water/archive/web/html/vms56.html*

[21]   Worsfold, P., McKelvie, I., Monbet, P., "Determination of phosphorus in natural waters: A historical review", *Analytica Chimica Acta*, Vol. 918, pp. 8–20, 2016.

[22]   Cordell, D., "A broken biogeochemical cycle", *Nature*, Vol. 478, pp. 29–31, 2011.

[23]   McPartlin, D.A., Lochhead, M.J., Connell, L.B., Doucette, G.J., O'Kennedy, R.J., "Use of biosensors for the detection of marine toxins", *Essays in Biochemistry*, Vol. 60, pp. 49–58, 2016.

[24]   Morabito, S., Silvestro, S., Faggio, C., "How the marine biotoxins affect human health", *Natural Product Research*, Vol. 32, pp. 621–631, 2018.

[25]   Gobler, C.J., Doherty, O.M., Hattenrath-Lehmann, T.K., Griffith, A.W., Kang, Y., Litaker, R.W., "Ocean warming since 1982 has expanded the niche of toxic algal blooms in the North Atlantic and North Pacific oceans", *Proceedings of the National Academy of Sciences*, Vol. 114, pp. 4975–4980, 2017.

[26]   Shim, K., Abdellatif, M., Park, J., Kim, D., "Antifouling effect of water-soluble phosphate glass frit for filtration plants", *Folia Microbiologica*, Vol. 65, pp. 363–370, 2020.

[27]   Gao, G., Yang, S., Xu, H., Dzakpasu, M., Jin, P., Wang, X.C., "Interception of sediment-liberated phosphate in a surface aquatic system for eutrophication control", *Water Supply*, Vol. 20, pp. 197–208, 2020.

[28]   Boyd, C.E., *Eutrophication*, Springer International Publishing, Cham, 2020.

[29]   Kundu, D., Roy, S.K., Dasgupta, S., "A rapid complexometric method for the determination of ZnO, Al 2 O 3 and P 2 O 5 in phosphate-based glasses", *Transactions of the Indian Ceramic Society*, Vol. 44, pp. 106–108, 1985.

[30]   Jain, K.K., *The Handbook of Nanomedicine*, Springer New York, New York, NY, 2017.

[31]   Bhushan, B., *Introduction to nanotechnology*, 2017.

[32]   Pham, X.H., Hahm, E., Huynh, K.H., Son, B.S., Kim, H.M., Jun, B.H., "Sensitive colorimetric detection of prostate specific antigen using a peroxidase-mimicking anti-PSA antibody coated Au nanoparticle", *Biochip Journal*, pp. 1–11, 2020.

[33]   Neely, A., Perry, C., Varisli, B., Singh, A.K., Arbneshi, T., Senapati, D., Kalluri, J.R., Ray, P.C., "Ultrasensitive and highly selective biomarker using two-photon rayleigh nanoparticle", *ACS nano*, Vol. 3, pp. 2834–2840, 2009.

[34]   Li, Y., Yuan, R., Chai, Y., Zhuo, Y., Su, H., Zhang, Y., "Horseradish peroxidase-loaded nanospheres attached to hollow gold nanoparticles as signal enhancers in an ultrasensitive immunoassay for alpha-fetoprotein", *Microchimica Acta*, Vol. 181, pp. 679–685, 2014.

[35]   Fan, P., Zhang, D., Wu, Y., Yu, J., Russell, T.P., "Polymer-modified ZnO nanoparticles as electron transport layer for polymer-based solar cells", *Advanced Functional Materials*, Vol. 30, pp. 2002932, 2020.

[36]   Fan, J., Cheng, Y., Sun, M., "Functionalized gold nanoparticles: synthesis, properties and biomedical applications", *The Chemical Record*, pp. tcr.202000087, 2020.

[37]   Dhal, S., Pal, K., Giri, S., "Transdermal delivery of gold nanoparticle by soybean oil-based oleogel under iontophoresis", *ACS Applied Bio Materials*, pp. acsabm.0c00893, 2020.

[38]   Borzenkov, M., Chirico, G., Pallavicini, P., Sperandeo, P., Polissi, A., Dacarro, G., Doveri, L., Collini, M., et al., "Nanocomposite sprayed films with photo-thermal

properties for remote bacteria eradication", *Nanomaterials*, Vol. 10, pp. 786, 2020.

[39] Stetsenko, M., Margitych, T., Kryvyi, S., Maksimenko, L., Hassan, A., Filonenko, S., Li, B., Qu, J., et al., "Gold nanoparticle self-aggregation on surface with 1,6-Hexanedithiol functionalization", *Nanomaterials*, Vol. 10, pp. 512, 2020.

[40] Pearson, R.G., "Hard and soft acids and bases", *Journal of the American Chemical Society*, Vol. 85, pp. 3533–3539, 1963.

[41] Ghosh, S.K., Nath, S., Kundu, S., Esumi, K., Pal, T., "Solvent and ligand effects on the ocalized Surface Plasmon Resonance (LSPR) of gold colloids", *The Journal of Physical Chemistry B*, Vol. 108, pp. 13963–13971, 2004.

[42] Prasad, B.L. V., Stoeva, S.I., Sorensen, C.M., Klabunde, K.J., "Digestive-ripening agents for gold nanoparticles: alternatives to thiols", *Chemistry of Materials*, Vol. 15, pp. 935–942, 2003.

[43] Cumberland, S.L., Strouse, G.F., "Analysis of the nature of oxyanion adsorption on gold nanomaterial surfaces", *Langmuir*, Vol. 18, pp. 269–276, 2002.

[44] Hu, X., Cheng, W., Wang, T., Wang, Y., Wang, E., Dong, S., "Fabrication, characterization, and application in SERS of self-assembled polyelectrolyte−gold nanorod multilayered films", *The Journal of Physical Chemistry B*, Vol. 109, pp. 19385–19389, 2005.

[45] Qu, Y., Lian, S., Shen, W., Li, Z., Yang, J., Zhang, H., "Rod-shaped gold nanoparticles biosynthesized using Pb2+-induced fungus Aspergillus sp. WL-Au", *Bioprocess and Biosystems Engineering*, Vol. 43, pp. 123–131, 2020.

[46] Fatehbasharzad, P., Stefania, R., Carrera, C., Hawala, I., Delli Castelli, D., Baroni, S., Colombo, M., Prosperi, D., et al., "Relaxometric studies of Gd-chelate conjugated on the surface of differently shaped gold nanoparticles", *Nanomaterials*, Vol. 10, pp. 1115, 2020.

[47] Rigó, I., Veres, M., Pápa, Z., Himics, L., Öcsi, R., Hakkel, O., Fürjes, P., "Plasmonic enhancement in gold coated inverse pyramid substrates with entrapped gold nanoparticles", *Journal of Quantitative Spectroscopy and Radiative Transfer*, Vol. 253, pp. 107128, 2020.

[48] Ghosh, S., Das, R., Kundu, S., Naskar, M.K., "Emulsion based solvothermal synthesis of CuO grainy rod via the formation of quasi-quadrangular prism shaped Cu2(OH)3Br for recyclable catalyst of 4-nitrophenol reduction", *Journal of Physics and Chemistry of Solids*, Vol. 147, pp. 109551, 2020.

[49] Faried, M., Ando, S., Suga, K., Okamoto, Y., Umakoshi, H., "Site specific analysis of anionic lipid by membrane surface-enhanced raman spectroscopy with different sized gold nanoparticles", *Chemistry Letters*, Vol. 49, pp. 1107–1110, 2020.

[50] Aiken, J.D., Finke, R.G., "A review of modern transition-metal nanoclusters: their synthesis, characterization, and applications in catalysis", *Journal of Molecular Catalysis A: Chemical*, Vol. 145, pp. 1–44, 1999.

[51] M. Christine Daniel, D.A., "Gold nanoparticles: assembly, supramolecular chemistry, quantum-size-related properties, and applications toward biology, catalysis, and nanotechnology"

[52] Couchman, P.R., Jessee, W.A., "Comments on the melting mechanism for crystalline

species", *Philosophical Magazine*, Vol. 35, pp. 787–790, 1977.

[53]   Piella, J., Bastús, N.G., Puntes, V., "Size-controlled synthesis of sub-10-nanometer citrate-stabilized gold nanoparticles and related optical properties.", *Chemistry of Materials*, Vol. 28, pp. 1066–1075, 2016.

[54]   Moballegh, A., Shahverdi, H.R., Aghababazadeh, R., Mirhabibi, A.R., "ZnO nanoparticles obtained by mechanochemical technique and the optical properties", *Surface Science*, Vol. 601, pp. 2850–2854, 2007.

[55]   He, Y.Q., Liu, S.P., Kong, L., Liu, Z.F., "A study on the sizes and concentrations of gold nanoparticles by spectra of absorption, resonance Rayleigh scattering and resonance non-linear scattering", *Spectrochimica Acta Part A: Molecular and Biomolecular Spectroscopy*, Vol. 61, pp. 2861–2866, 2005.

[56]   Perezjuste, J., Pastorizasantos, I., Lizmarzan, L., Mulvaney, P., "Gold nanorods: Synthesis, characterization and applications", *Coordination Chemistry Reviews*, Vol. 249, pp. 1870–1901, 2005.

[57]   Hutter, E., Fendler, J.H., "Exploitation of localized surface plasmon resonance", *Advanced Materials*, Vol. 16, pp. 1685–1706, 2004.

[58]   Ghosh, S.K., Pal, T., "Interparticle Coupling Effect on the Surface Plasmon Resonance of Gold Nanoparticles: From Theory to Applications", *Chemical Reviews*, Vol. 107, pp. 4797–4862, 2007.

[59]   Zhang, J.Z., Noguez, C., "Plasmonic optical properties and applications of metal nanostructures", *Plasmonics*, Vol. 3, pp. 127–150, 2008.

[60] Pelton, M., Aizpurua, J., Bryant, G., "Metal-nanoparticle plasmonics", *Laser & Photonics Review*, Vol. 2, pp. 136–159, 2008.

[61] Sau, T.K., Rogach, A.L., Jäckel, F., Klar, T.A., Feldmann, J., "Properties and applications of colloidal nonspherical noble metal nanoparticles", *Advanced Materials*, Vol. 22, pp. 1805–1825, 2010.

[62] Murray, W.A., Barnes, W.L., "Plasmonic materials", *Advanced Materials*, Vol. 19, pp. 3771–3782, 2007.

[63] Sze, S.M., Ng, K.K., *Physics of semiconductor devices*, John Wiley & Sons, Inc., Hoboken, NJ, USA, 2006.

[64] Rotello, V., *Nanoparticles building blocks for nanotechnology*, Springer, USA, 2004.

[65] Yguerabide, J., Yguerabide, E.E., "Light-scattering submicroscopic particles as highly fluorescent analogs and their use as tracer labels in clinical and biological applications", *Analytical Biochemistry*, Vol. 262, pp. 157–176, 1998.

[66] Nguyen, D.T., Kim, D.-J., So, M.G., Kim, K.-S., "Experimental measurements of gold nanoparticle nucleation and growth by citrate reduction of HAuCl4", *Advanced Powder Technology*, Vol. 21, pp. 111–118, 2010.

[67] Daruich De Souza, C., Ribeiro Nogueira, B., Rostelato, M.E.C.M., "Review of the methodologies used in the synthesis gold nanoparticles by chemical reduction", *Journal of Alloys and Compounds*, Vol. 798, pp. 714–740, 2019.

[68] Araki, K., Mizuguchi, E., Tanaka, H., Ogawa, T., "Preparation of very reactive thiol-protected gold nanoparticles: revisiting the brust-schiffrin method", *Journal of*

Nanoscience and Nanotechnology, Vol. 6, pp. 708–712, 2006.

[69] Frenkel, A.I., Nemzer, S., Pister, I., Soussan, L., Harris, T., Sun, Y., Rafailovich, M.H., "Size-controlled synthesis and characterization of thiol-stabilized gold nanoparticles", *The Journal of Chemical Physics*, Vol. 123, pp. 184701, 2005.

[70] Leff, D. V., Brandt, L., Heath, J.R., "Synthesis and characterization of hydrophobic, organically-soluble gold nanocrystals functionalized with primary amines", *Langmuir*, Vol. 12, pp. 4723–4730, 1996.

[71] Sardar, R., Bjorge, N.S., Shumaker-Parry, J.S., "pH-controlled asemblies of polymeric amine-stabilized gold nanoparticles", *Macromolecules*, Vol. 41, pp. 4347–4352, 2008.

[72] Rak, M.J., Saadé, N.K., Friščić, T., Moores, A., "Mechanosynthesis of ultra-small monodisperse amine-stabilized gold nanoparticles with controllable size", *Green Chem.*, Vol. 16, pp. 86–89, 2014.

[73] Gandubert, V.J., Lennox, R.B., "Assessment of 4-(Dimethylamino)pyridine as a capping agent for gold nanoparticles", *Langmuir*, Vol. 21, pp. 6532–6539, 2005.

[74] Kang, S.W., Hong, J., Park, J.H., Mun, S.H., Kim, J.H., Cho, J., Char, K., Kang, Y.S., "Nanocomposite membranes containing positively polarized gold nanoparticles for facilitated olefin transport", *Journal of Membrane Science*, Vol. 321, pp. 90–93, 2008.

[75] Kamimura, A., Yamada, K., Kuratani, T., Oishi, Y., Watanabe, T., Yoshida, T., Tomonaga, F., "DMAP as an effective catalyst To accelerate the solubilization of waste fiber-reinforced plastics", *ChemSusChem*, Vol. 1, pp. 845–850, 2008.

[76] Halder, J., Islam, N., "Water pollution and its impact on the human health", *Journal of*

Environment and Human, Vol. 2, pp. 36–46, 2015.

[77] Schwarzenbach, R.P., Egli, T., Hofstetter, T.B., von Gunten, U., Wehrli, B., "Global water pollution and human health", *Annual Review of Environment and Resources*, Vol. 35, pp. 109–136, 2010.

[78] Dojlido, J. ; Best, G.A., *Chemistry of water and water pollution.*, Ellis Horwood Limited, 1993.

[79] Kumar, V., Sharma, A., Kumar, R., Bhardwaj, R., Kumar Thukral, A., Rodrigo-Comino, J., "Assessment of heavy-metal pollution in three different Indian water bodies by combination of multivariate analysis and water pollution indices", *Human and Ecological Risk Assessment: An International Journal*, Vol. 26, pp. 1–16, 2020.

[80] Saleh, I.A., Zouari, N., Al-Ghouti, M.A., "Removal of pesticides from water and wastewater: Chemical, physical and biological treatment approaches", *Environmental Technology & Innovation*, Vol. 19, pp. 101026, 2020.

[81] Xu, R., Cai, Y., Wang, X., Li, C., Liu, Q., Yang, Z., "Agricultural nitrogen flow in a reservoir watershed and its implications for water pollution mitigation", *Journal of Cleaner Production*, Vol. 267, pp. 122034, 2020.

[82] Ma, C., Xiao, Y., Puig-Bargués, J., Shukla, M.K., Tang, X., Hou, P., Li, Y., "Using phosphate fertilizer to reduce emitter clogging of drip fertigation systems with high salinity water", *Journal of Environmental Management*, Vol. 263, pp. 110366, 2020.

[83] D'Itri, F.M., "Environmental mercury problem", 1972.

[84] Chen, G.-H., Chen, W.-Y., Yen, Y.-C., Wang, C.-W., Chang, H.-T., Chen, C.-F.,

"Detection of mercury(II) ions using colorimetric gold nanoparticles on paper-based analytical devices", *Analytical Chemistry*, Vol. 86, pp. 6843–6849, 2014.

[85] Khosraviani, M., Pavlov, A.R., Flowers, G.C., Blake, D.A., "Detection of heavy metals by immunoassay: Optimization and validation of a rapid, portable assay for ionic cadmium", *Environmental Science & Technology*, Vol. 32, pp. 137–142, 1998.

[86] Kasuya, M., Teranishi, H., Aoshima, K., Katoh, T., Horiguchi, H., Morikawa, Y., Nishijo, M., Iwata, K., "Water pollution by cadmium and the onset of Itai-itai disease", *Water Science and Technology*, Vol. 25, pp. 149–156, 1992.

[87] Vinot, H., Larpent, J.P., "Water pollution by uranium ore treatment works", *Hydrobiologia*, Vol. 112, pp. 125–129, 1984.

[88] Kurttio, P., Auvinen, A., Salonen, L., Saha, H., Pekkanen, J., Mäkeläinen, I., Väisänen, S.B., Penttilä, I.M., et al., "Renal effects of uranium in drinking water.", *Environmental Health Perspectives*, Vol. 110, pp. 337–342, 2002.

[89] Naderi, M., Hosseini, M., Ganjali, M.R., "Naked-eye detection of potassium ions in a novel gold nanoparticle aggregation-based aptasensor", *Spectrochimica Acta Part A: Molecular and Biomolecular Spectroscopy*, Vol. 195, pp. 75–83, 2018.

[90] Wu, J., Babcock, B.A., "Metamodeling potential nitrate water pollution in the central United States", *Journal of Environmental Quality*, Vol. 28, pp. 1916–1928, 1999.

[91] Walker, W.H., "Ground-water nitrate pollution in rural areas", *Ground Water*, Vol. 11, pp. 19–22, 1973.

[92] Hecky, R.E., "The eutrophication of lake Victoria", *SIL Proceedings, 1922-2010*, Vol. 25,

pp. 39–48, 1993.

[93]   Harper, D., *Eutrophication of freshwaters*, Springer Netherlands, Dordrecht, 1992.

[94]   Jørgensen, S.E., "A eutrophication model for a lake", *Ecological Modelling*, Vol. 2, pp. 147–165, 1976.

[95]   Kimling, J., Maier, M., Okenve, B., Kotaidis, V., Ballot, H., Plech, A., "Turkevich method for gold nanoparticle synthesis revisited", *The Journal of Physical Chemistry B*, Vol. 110, pp. 15700–15707, 2006.

APPENDIX

In this section, paper-based sensor and tablet-based gold nanoparticle investigated. However, these formats were not successful and moved to appendix section.

A. Fabrication of a paper-based sensor

To find the functionality of MA-AuNPs on paper platform as a paper-based microfluidic sensor, different paper substrates including regular office paper, Whatman filter paper grades #1, #2, and #4 were tested. Commercialized office papers are often treated to optimize the applicability in writing with different inks; hence, these papers are hydrophobic to some extent. To test this office paper, MA-AuNPs was dropped on the paper using micropipette and solution of Eu^{3+} was added to the gold drop on the paper. After addition of Eu^{3+} solution to the MA-AuNPs, the resulting mixture got absorbed by the paper after 1 min. Based on the observation, the reference reaction zone which was MA-AuNPs alone turned dark blue before paper absorption and as it is shown in Fig. 27 both reaction spots have the same colors. To change the environment of the paper, the paper was dipped in the tris-buffer HCl with the pH of 7.4 and let to air-dry. However, based on the Fig. 27, the result was not different and by dropping the MA-AuNPs solution on the paper, the color changed to dark blue and absorbed by the paper after 1 min. As a result, commercialized treated papers are not the right choice for this aim.
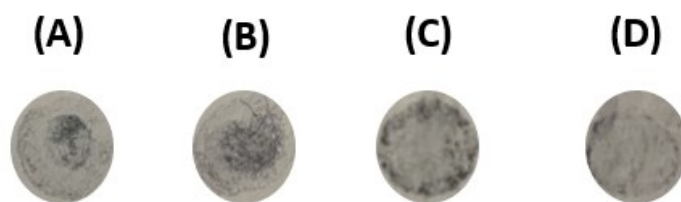
Fig. 27 Results of commercialized treated paper for sensor applications. (A) MA-AuNPs reference drop on the unwashed A4 paper (B) MA-AuNPs and Eu³⁺ drop on the unwashed A4 paper (C) MA-AuNPs reference drop on the washed A4 paper (D) MA-AuNPs and Eu³⁺ drop on the unwashed A4 paper.

Whatman filter paper #1 and filter paper #2 were tested by dropping MA-AuNPs as a spot test (Fig. 28). Since these papers were not pre-treated, they were not hydrophobic, and the drops were absorbed immediately after addition. However, the results were not promising as the MA-AuNPs (red) changed to blue without the addition of any extra reagent (Eu³⁺ nor Pi). Moreover, changing the pH of the paper by dipping the paper in the tris-buffer HCl (pH 7.4) was not successful and gave the same result.
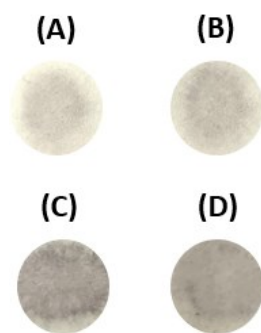

Fig. 28 Whatman filter paper grades #1 and #2 results. (A) MA-AuNPs reference spot on the Whatman #1, (B) mixture of MA-AuNPs and Eu³⁺ solution on Whatman #1, (C) MA-AuNPs reference spot on the Whatman #2 (D) mixture of MA-AuNPs and Eu³⁺ solution on Whatman #2.

For filter paper Whatman #4, 9 µL of MA-AuNPs was dropped on a spot, a circular pink area was created, and the pink color was stable even when the solution dried on the paper. To test

the aggregation effect, 3 µL of Eu^{3+} (220 µM) was dropped on the paper. Based on the presented investigations, filter paper Whatman #4 had the best results in terms of MA-AuNPs color stability on the paper. However, Whatman paper had the mixing issue since its fibres reduced the MA-AuNPs and Eu^{3+} mobility.
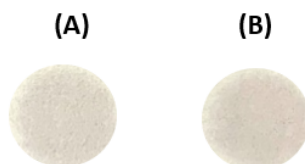
(A)   (B)

Fig. 29 Test results of filter paper Whatman #4. (A) The reference MA-AuNPs zone, (B) The mixture of MA-AuNPs and Eu^{3+} solution.

Another method was deployed to allow mixing of the reagents on the paper, this was done by dipping the paper in the target's solution bath so it can flow laterally. This experiment let Eu^{3+} and MA-AuNPs mix when the solution is flowing up in the paper-based device. However, on drying the solution on the paper, the MA-AuNPs turns dark blue which means it is not stable for a long time.

In all, all the paper-based devices that were fabricated for the detection assay did not provide any enough color change and stability for phosphate detection in water. Therefore, the paper-based sensor was not used going forward, and a tablet-based approach was investigated.

B. Fabrication of a tablet-based MA-AuNPs

Dextran/pullulan-MA-AuNPs tablets (Fig. 30) were prepared and its efficiency was observed. However, dissolving the dextran/pullulan-MA-AuNPs tablets didn't give the desired color changes. This poor performance can be linked to the shielding of the MA-AuNPs by the

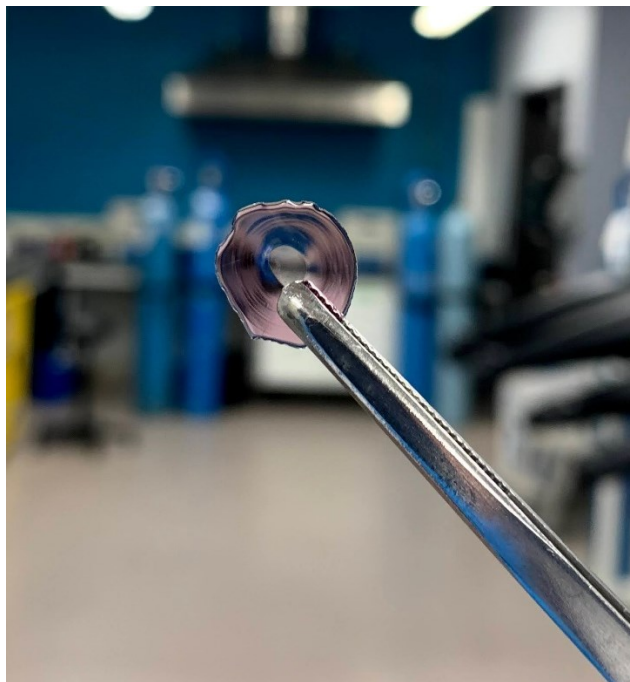polymer molecules which could disturb its appropriate electrostatic feature, therefore causing a loss of activity.

Fig. 30 MA-AuNPs dextran tablet.